GULF GENERAL ATOMIC

Gulf-GA-A12824
UC-77 Gas Cooled Reactor
Technology

GAS-COOLED FAST BREEDER REACTOR

QUARTERLY PROGRESS REPORT

FOR THE PERIOD AUGUST 1, 1973 THROUGH OCTOBER 31, 1973

by

Project Staff

Prepared for the
U.S. Atomic Energy Commission
San Francisco Operations Office
Under
Contract AT(04-3)-167
Project Agreement No. 23

Gulf General Atomic Project 393 December 10, 1973

GULF GENERAL ATOMIC COMPANY
P.O. BOX 81608, SAN DIEGO, CALIFORNIA 92138

PROGRESS REPORT SERIES

GA-5537	November 1, 1963 to July 31, 1964
GA-6667	August 1, 1964 to July 31, 1965
GA-7645	August 1, 1965 to July 31, 1966
GA-8107	August 1, 1966 to July 31, 1967
GA-8787	August 1, 1967 to July 31, 1968
GA-8895	August 1, 1968 through October 31, 1968
GA-9229	November 1, 1968 through January 31, 1969
GA-9359	February 1, 1969 through April 30, 1969
GA-9639	May 1, 1969 through July 31, 1969
GA-9811	August 1, 1969 through October 31, 1969
GA-9838	November 1, 1969 through January 31, 1970
GA-10517	February 1, 1970 through January 31, 1971
GA-10645	February 1, 1971 through April 30, 1971
GA-A10803	May 1, 1971 through July 31, 1971
GA-A10906	August 1, 1971 through October 31, 1971
GA-A12003	November 1, 1971 through January 31, 1972
GA-A12165	February 1, 1972 through April 30, 1972
GA-A12252	May 1, 1972 through July 31, 1972
GA-A12421	August 1, 1972 through October 31, 1972
GA-A12530	November 1, 1972 through January 31, 1973
GA-A12635	February 1, 1973 through April 30, 1973
GA-A12728	May 1, 1973 through July 31, 1973

ABSTRACT

The tasks of the Gas-Cooled Fast Breeder (GCFR) program that are supported by the U.S. Atomic Energy Commission are program planning, core development, out-of-pile heat-transfer and fluid-flow tests, development of a pressure-equalization system for fuel rods, fuels and materials development, and nuclear analysis and reactor physics.

The core development task is to establish criteria for the design of the GCFR fuel, control, and blanket element assemblies. Analytical methods are being developed for predicting fuel-rod response to transient conditions and for treating thermal-hydraulic and structural analyses of fuel assemblies. For the heat-transfer and fluid-flow tests of fuel assemblies, planning of the test program and test facility was initiated. The development work on the pressure-equalization system included designing the test assemblies for static adhesion tests and seal leakage tests, development of the fuel-rod manifold, and development of an analytical model for designing monitoring instrumentation. In the fuels and materials task, the status of the thermal and fast-flux irradiation programs and analyses of data from these experiments is given. Nuclear analysis and reactor physics work included GCFR critical experiment planning, surveillance of LMFBR critical assembly experiments, and methods development.

CONTENTS

Figures

Tables

1. INTRODUCTION

The Gas-Cooled Fast Breeder Reactor (GCFR) program sponsored by the U.S. Atomic Energy Commission consists of six tasks: Task 1000—Program Planning, Task 4100—Core Development, Task 4120—Fuel and Blanket Element Assemblies, Task 4160—Pressure Equalization System for Fuel, Task 4200/4400—Fuels and Materials Development, and Task 4700—Nuclear Analysis and Reactor Physics. The broad objectives of each of these tasks and a summary of the work accomplished in each task during the period covered by this report are given in this section. The technical work performed on the GCFR program during this reporting period is presented in Sections 2 through 5.

The GCFR Utility Program, which is supported by a large number of electric utility companies, rural electric cooperatives, and Gulf General Atomic, is primarily directed toward the development of a 300-MW(e) GCFR demonstration plant. This utility-sponsored work and the AEC-sponsored work are complementary.

1.1. TASK 1000—PROGRAM PLANNING

This task is primarily to coordinate the planning and implementing of the tasks for the technical development of the GCFR. This task also includes liaison with Argonne National Laboratory (ANL) and Oak Ridge National Laboratory (ORNL) on the safety programs they are performing under AEC funding; the corresponding safety program at Gulf General Atomic is privately funded.

This task is primarily administrative and thus only the technical work performed during this period is covered in this quarterly report.

1.2. TASK 4100—CORE DEVELOPMENT

The objective of this task is the engineering development of the reactor core and associated components. The work on this task is directed

specifically to establishing criteria for the design of the fuel and blanket element assemblies. The various analytical and experimental investigations being carried out on this task are reported in Section 2.

As part of a survey of methods available to perform transient fuel-rod analysis, an evaluation was made of the conditions under which a series of steady-state calculations could provide an adequate evaluation of the GCFR fuel-rod response to transients. These transients, which include startup, shutdown, and changes in reactor power, will be treated with the LIFE-II code as a succession of steady power conditions.

In the analysis of fuel- and blanket-element assemblies, preparations were made to have Battelle Pacific Northwest Laboratories perform a stress analysis of the fuel-rod spacer-grid structure for several loading conditions. At GGA a dynamic analysis model of the movement of the spacer grid relative to the fuel rods and duct wall has been defined. The model consists of two fuel rods at opposite edges of the assembly, the spacer-grid hangers, and the duct wall.

Interaction diagrams and fault trees developed for designing and analyzing LMFBR fuel elements were modified for application to the GCFR fuel elements. However, it was found that for the GCFR concept, new fault trees would have to be developed.

In the analytical studies of GCFR elements, improvements in the calculation methods applicable to the helium-cooled elements have been made in HETHRA to include the improved cross-flow algorithm in COBRA-IIIC and to increase the capacity of the code.

The behavior of surface-roughened and smooth-surface fuel-rod cladding tubes moving axially relative to a section of the spacer grid is being investigated experimentally. Tests performed on surface-roughened (ribbed) tubes at 525°C indicated wear on the ribs and on the dimples of the spacer grid that may have been due to misalignment of the test samples. Tests were made on smooth tubes to evaluate the effect of helium impurities on performance. It was found that the spacers adhered to the smooth tube when tested in 90 μatm H_2O and 900 μatm H_2 at 525°C. This behavior is being analyzed in further tests.

1.3. TASK 4120—FUEL- AND BLANKET-ELEMENT ASSEMBLIES

A series of out-of-pile heat-transfer and fluid-flow tests will be performed to demonstrate the ability of the GCFR fuel, control, and blanket element designs to meet design goals and to verify predictions of analytical models that describe design operation and accident behavior. Heat-transfer and fluid-flow data will be obtained using electrically heated rod bundles in a dynamic helium loop. The test objectives and preliminary test requirements are discussed in Section 3.

This test program is to be carried out jointly by GGA and ORNL. During this reporting period, a coordinating committee was formed, the objectives of the test program were defined, the areas of responsibility were established, and joint schedules for the overall program and for FY 74 were initiated. The test facility that will be used to conduct the heat-transfer and fluid-flow tests will be at ORNL and has been designated the Core Flow Test Facility (CFTF).

1.4. TASK 4160—PRESSURE EQUALIZATION SYSTEM FOR FUEL

The objective of this task is to develop a system for equalizing the pressure between the inside and the outside of the GCFR fuel rod and for venting the fission products via a trapping system and an instrumented activity monitoring system to a helium purification system. The work performed on this task during this reporting period is presented in Section 4.

In the test program for developing the element-to-grid plate and vent-connection seal, work in progress included designing the test assemblies for the static adhesion tests of grid-plate and element parts and for the vent-connection seal leakage test and preparing the test plans.

To obtain data for developing the monitoring system and instrumentation for the pressure equalization system, a Ge(Li) analyzer is being developed for installation on the sweep-gas line of the GB-10 capsule that is being irradiated in the ORR. The computer program COUNT, which is being used in the design of the Ge(Li) analyzer, is being developed to obtain information on fission products during leaking-element conditions.

Design criteria have been established for the fission-product manifold, design studies were made of one-level and two-level manifold concepts, and plans were prepared for testing metal-to-metal seals that are to be used for connecting the fuel rods to the manifold.

1.5. TASK 4200/4400—FUELS AND MATERIALS DEVELOPMENT

The fuels and materials development and testing program extends and applies Liquid-Metal Fast Breeder Reactor (LMFBR) fuel technology to GCFR requirements. This task includes surveillance of the LMFBR fuels and materials program to utilize existing and developing technology applicable to the GCFR. The status of the GCFR thermal-flux and fast-flux irradiation test programs is presented in Section 5.

Postirradiation examination of capsule GB-9 was continued with the receipt at GGA of the charcoal trap, cladding specimens, and dosimetry monitors. The intact charcoal trap was gamma-scanned for fission-product activity and then the charcoal was removed in axial sections for detailed isotopic iodine and cesium analyses.

Irradiation of capsule GB-10 was resumed after the scheduled shutdown of the ORR in August. The capsule was operating at a power level of 13.5 kW/ft and a cladding outer surface temperature of 565°C when a leak occurred at a valve in the sweep-gas line of the capsule assembly. The capsule will be reinserted in the ORR for continued irradiation after the leaking valve has been repaired during the next ORR refueling shutdown. At the time the capsule assembly was retracted from the ORR because of the leak, the GB-10 fuel rod had reached a burnup of ~29,700 MWd/Te.

Data on GB-10 operation covering a period of approximately one year have been received from ORNL.

The second interim examination of the seven encapsulated fuel rods in the F-1 fast-flux irradiation experiment was completed after burnup exposures up to 56,000 MWd/Te had been reached. The five fuel rods removed from the subassembly were shipped to ANL-East for destructive examination. The F-1 (X094B) subassembly with the five new encapsulated fuel rods will be reinserted in EBR-II for continued irradiation of the one remaining initial fuel rod to a burnup goal of 100,000 MWd/Te.

Analysis of the data obtained during the second interim examination of the F-1 fuel rods is continuing at GGA. Analysis of diametral scans of rods G-1, G-4, and G-8 has been completed. Supplemental gamma-scanning at 0.5-in. intervals was made along the length of rod G-8. These data will be compared with similar axial scans made on rods G-3 and G-4 during the first interim examination at 25,000 MWd/Te.

Postirradiation examination of rod G-3 is continuing. Samples of the G-3 fuel-rod cladding are being used at GGA to determine the actual operating temperature during irradiation using the Kr^{85} annealing technique. Plenum-gas analysis and volume measurements made at ANL-East indicate that the G-3 plenum volume was approximately the same as the calculated volume.

The fabrication and assembly of the F-3 fast-flux experiment is continuing. Minor modifications were made to the lower end fittings of rods G-16 and G-17 to facilitate their being incorporated into a transient test assembly after the F-3 experiment is complete. Subcapsules containing neutron shielding materials were fabricated and shipped to ANL-East. The assembly of one fuel rod, except the xenon tagging, has been completed by ANL.

1.6. TASK 4700—NUCLEAR ANALYSIS AND REACTOR PHYSICS

This task involves the surveillance and analyses of LMFBR physics work and critical experiments to properly coordinate and develop a GCFR nuclear analysis and physics program and the design and planning of a GCFR critical experiment program. The work performed under this task during this reporting period is discussed in Section 6.

Surveillance of LMFBR critical assembly experiments continued with the objective of establishing an experimentally verified basis for GCFR reactor physics work. Reanalysis of ZPPR-2 central worths in the voided inner core is being made with ENDF/B Version 3 cross sections. First-order perturbation worths were calculated. The effect on central worths of extending the resolved resonance treatment from 3 keV to 7.1 keV was also examined. Work on the development of analytical methods continued. Planning for the GCFR critical assembly experiment included reviewing a preliminary work plan prepared by the Applied Physics Division, Argonne National Laboratory.

2. TASK 4100—CORE DEVELOPMENT

2.1. FUEL- AND BLANKET-ROD ANALYSIS

As part of a survey of methods available to perform transient fuel-rod analysis, an evaluation was made of the transient conditions under which a series of steady-state calculations could provide an adequate evaluation of the fuel-rod response to transients. This is appropriate since most of the GCFR operational transients and even accident transients, such as design-basis depressurization, are relatively slow. Faster transients require a direct time integration, and computer codes that perform this type of analysis are in the developmental stages.

Using the LIFE-II code, which is a steady-state code with respect to instantaneous fuel temperatures, transient conditions such as startup, shutdown, and changes in power level can be treated as a succession of steady power conditions by the use of history cards. Results for single rods should be valid if the time intervals on the history cards are appreciably longer than the relaxation time for the internal temperature change in the rod. In addition, a core transient can be treated as a succession of steady states if the duration of each state is appreciably longer than the relaxation time for the core as a whole to approach a new equilibrium condition.

The fuel rod can be considered as an infinite solid cylinder with conduction from the fuel surface through a gas gap to the cladding. Neglecting the time constant of the cladding itself, the relaxation time, τ, of the rod is given by

$$\tau = \frac{\rho\, c\, r^2}{k\, S_n^2} \quad ,$$

where ρ = fuel density,

c = fuel heat capacity,

r = fuel-rod radius,

k = fuel conductivity,

S_n = dimensionless constant.

The constant S_n is the root[1] of

$$S_n J_1(S_n) = A J_0(S_n),$$

where $A = \frac{rh}{k}$,

h = fuel-surface-to-cladding conductance.

Using typical values for a GCFR fuel rod,

$r = 0.4$ cm,

$h = 1.0$ W/cm^2-°C,

$k = 0.02$ W/cm-°C

$C = 0.25$ J/g-°C,

$\rho = 10$ g/cm^3,

we have

$$A = 0.4 \times 1.0/0.02 = 20$$

and

$$S_1 = 2.288.$$

This is close enough to the root (2.405) of $J_0(S_1) = 0$ that the thermal resistance between fuel and cladding can be neglected in determining the relaxation time for internal conduction. With these values, the relaxation time for conduction would be

$$\tau = \frac{10 \times 0.25 \times (0.4)^2}{0.02 \times (2.288)^2} = 3.82 \text{ sec.}$$

Thus, transients that can be approximated by a succession of steady states of 5- to 10-sec duration could be treated using the LIFE-II code. These transients include normal operational power changes but not a reactor scram. They also include accident transients, such as depressurization.

The rate of approach of the core to a new temperature distribution following a change in boundary conditions can be estimated using transient heat-exchanger calculations. The number of transfer units for heat exchangers is

$$N = \frac{hA}{WC_p} ,$$

where h = average heat-transfer coefficient,

A = total heat-exchange area,

W = coolant flow rate,

C_p = coolant heat capacity,

and the time to achieve a given temperature approach to equilibrium is

$$t = \phi \frac{W_s C_s}{WC_p} ,$$

where W_s = total structure weight in core,

C_s = average structure heat capacity,

and ϕ is determined from Fig. 2.1 for a given value of N and the desired dimensionless temperature approach X.

For example, a typical GCFR core has a value of N = 2.3 transfer units. The core material includes 8.73×10^6 g of fuel having a heat capacity of about 0.25 J/g-°C and 3.7×10^6 g of steel having a heat capacity of about 0.4 J/g-°C. The gas flow rate is 0.703×10^6 g/sec with a heat capacity of 5.2 J/g-°C. The time is therefore given by

$$t = \phi \left[\frac{(8.73 \times 10^6) \times 0.25 + (3.7 \times 10^6) \times 0.4}{(0.703 \times 10^6) \times 5.2} \right]$$

$$= 1.00 \phi \text{ sec.}$$

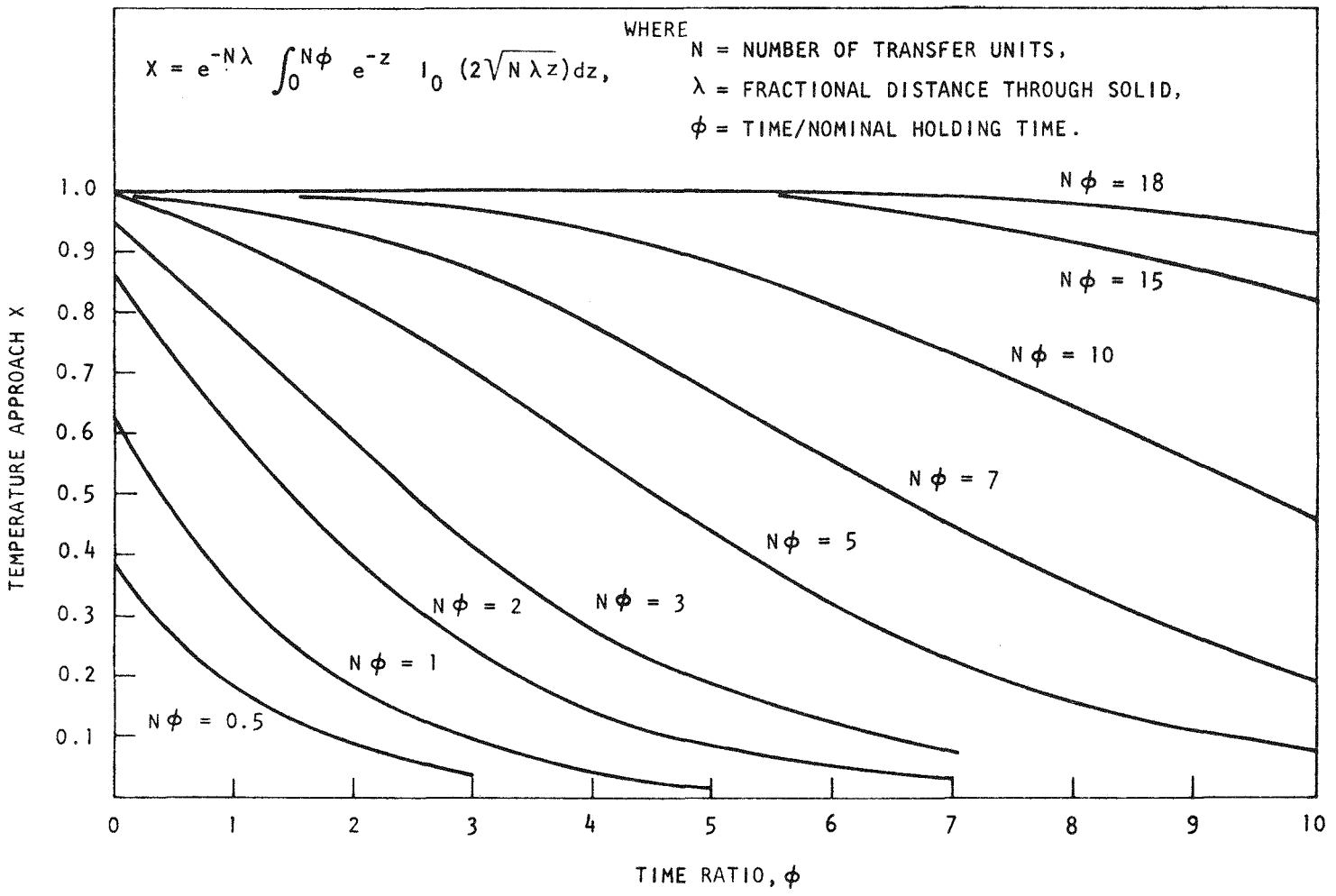

Fig. 2.1 Solid temperature transient heating curves

Referring to Fig. 2.1, at values of $\lambda = 1$ (outlet end of core), $N = 2.3$, and $X = 0.8$ (80% temperature approach), $N\phi = 5.1$ or $\phi = 2.22$. Thus the 80% approach time, t, is 2.22 sec.

The core transient heat transfer can be handled as a succession of steady-state temperature calculations if the history can be approximated by steady-state intervals of 5- to 10-sec duration. Transients much faster than this will require a more sophisticated definition of the core temperature distribution and the use of a true transient code for the fuel-rod behavior, such as SAS2A. Possibly the temperature calculation part of SAS2A could be used with LIFE-II to get a somewhat better approximation for instantaneous fuel temperatures.

2.2. ANALYSES OF FUEL- AND BLANKET-ELEMENT ASSEMBLIES

2.2.1. Analysis of Fuel-rod–Spacer Interaction

The purpose of this subtask is to perform a stress analysis of the fuel-rod spacer-grid structure for several loading conditions imposed on the spacer grid by the fuel rods. These loads result from fuel-rod bowing that is due to temperature gradients across the rods and from irradiation-induced swelling and creep. They consist of both a lateral load and a friction-induced axial load that occurs if the rod moves relative to the grid. The work on this subtask is to be performed under subcontract by Battelle Pacific Northwest Laboratories.

The spacer-grid structure is to be modeled by plate-type finite elements and the calculations are to be made using finite-element structural-analysis computer codes. The model development and analysis of the fuel-rod spacer grid will include:

1. A one-twelfth segment of the spacer grid with a constant wall thickness for constant-axial-load elastic analysis (load caused by thermal transient).
2. A segment of unit cell deflection, including thermal- and irradiation-induced creep, which results from a lateral time-dependent load (load caused by fuel-rod bowing).

3. Axial buckling of the spacer-grid support hanger for constant axial load (load caused by thermal transient).

4. Initiation of an analysis of a half-segment of spacer grid for summation of lateral fuel-rod loads: (a) flat (flat channel) and (b) point (point channel).

2.2.2. Analysis of Duct-wall Behavior

The model used in the previous calculations of duct dilation and bowing was reviewed. This model will be modified to include the effect of the spacer-grid hangers that act as an internal insulation for the duct wall and for the flow external to the duct caused by aspiration that results from the coolant flow out of the bottom of the assemblies. Both these effects tend to reduce the temperature gradient across the duct.

Duct dilation calculations will be made with the MARC computer code. An initial model of the duct wall that included flat and curved corner sections of the duct but using only 39 finite elements was calculated. A model with a larger number of finite elements will be required to fully define the deflections and bending stress. The September 1973 irradiation-induced swelling and creep correlations[2] of the Ad Hoc Committee will be incorporated in these calculations.

2.2.3. Analysis of Spacer-grid Mounting

A dynamic analysis model of the movement of the spacer grid relative to the fuel rods and duct wall has been defined. The purpose of the analysis is to determine the relative axial motion between the spacer grid and fuel rods during a transient. The model will also determine the transient bow and lateral motion of the duct for the case where a radial power gradient exists. The effect of heat transfer between adjacent ducts will be evaluated. The model consists of two fuel rods at opposite edges of the assembly, the spacer-grid hangers, and the duct wall. The model is divided into eight axial sections. Each axial section of fuel rod has a fuel node, two cladding nodes, and two coolant channels to provide a mixing adjustment for coolant and cladding temperatures. The hanger and duct each represent a node with connecting conductance and each with convective heat transfer to an adjacent

coolant channel. Thus, each axial section consists of ten nodes. Power and flow transients are introduced and node transient temperatures are computed. These temperatures are then used to calculate the transient motion of the assembly. The coding of the model has been completed and a compilation of the program prepared. A test program will be run to determine equilibrium temperatures to be used as initial conditions and to ensure that all of the node interconnections are correct.

2.2.4. Graphical Presentation, Design Criteria, and Data Base

Interaction diagrams and fault-tree analysis[3] have proven to be useful in the design and analysis of the fuel elements for the LMFBR.[4,5] The objective of such an analysis is to show the relationships that are operative in the design of fuel, control, and blanket elements and thereby to determine sensitive problem areas. This mechanistic approach is used to gain an understanding of the possible behavior of the elements during off-normal and accident conditions and to identify what test data and analyses are necessary to establish the transition from one condition to the next.

An incremental approach to the development of a fault tree for the GCFR fuel element design was tried by modifying existing LMFBR fault trees to reflect GCFR conditions. The modification consisted mainly of eliminating effects associated with sodium and with the relatively high fission-gas pressure in LMFBR fuel rods. Fission-gas pressure is eliminated in the GCFR by the pressure equalization system, which maintains a small (< 20 psi) pressure difference across the fuel-rod cladding. However, even with the elimination of these two effects, the remaining branches of the fault tree did not result in a useful diagram of possible GCFR fault paths. Consequently, new fault trees will be generated for the GCFR core, with particular attention directed toward the more probable fault paths associated with the GCFR fuel-element concept.

2.2.5. Method Improvement and Verification

The HETHRA code was developed from COBRA-II to treat the GCFR helium-cooled element. The improved COBRA-IIIC was received in May, 1973, and HETHRA

has since been modified to include the improved cross-flow algorithm in COBRA-IIIC. This modification is called COBRA-G for gas. Two test cases were run to compare the predictions of COBRA-G with those of the original HETHRA. The first test case was a 7-rod bundle with uniform heating and no distortion and the second test case was a 7-rod bundle with uniform heating and a 10-mil bow in the center rod. The two test cases indicated that the small oscillation in the cross flow in the HETHRA results was damped out in the COBRA-G calculation. The temperature predictions with HETHRA and COBRA-G are compared in Table 2.1. The case with no distortion shows almost no temperature difference, whereas the case with a 10-mil rod bow indicates a 7.3°F increase in the maximum cladding temperature. Downstream from the position of maximum bow, the predicted flow recovery is slower in the COBRA-G, which results in an increase in the predicted temperature. Further study of the cross-flow calculation is planned to determine whether this temperature increase is reasonable.

At the same time that the cross-flow algorithm was improved, the capacity of the code was increased to handle a 61-rod bundle with 150 subchannels and 202 cross connections. Although a 61-rod bundle has 210 cross connections, only 202 can be accommodated in the computer core storage at GGA. After the GGA computer core storage has been expanded, a complete 61-rod hexagonal bundle can be computed. Further expansion is dependent on modifying the cross-flow matrix algorithm.

2.3. FUEL-ROD—SPACER-GRID INTERACTION TESTS

In these tests, the behavior of a surface-roughened (ribbed) fuel rod and a smooth-surface fuel rod moving axially relative to a section of the spacer grid is being investigated. The information being sought is the adequacy of the design and the range of impurities in the GCFR helium coolant over which acceptable performance is obtained. The test objectives and apparatus have been previously discussed in the last quarterly report.[6] During this reporting period, further tests were made at 525°C, the second test fixture and an all-welded stainless-steel gas supply system were completed, and time-temperature stability tests were made of spacer-grid dimples at test temperatures.

Table 2.1

COMPARISON OF HETHRA AND COBRA-G TEMPERATURE PREDICTIONS FOR 7-ROD BUNDLE

Parameter	No Distortion		10-mil Rod Bow	
	HETHRA	COBRA-G	HETHRA	COBRA-G
Average outlet temperature, °F	1007.5	1007.5	1007.5	1007.5
Maximum outlet temperature, °F	1017.2	1017.5	1020.8	1024.5
Minimum outlet temperature, °F	995.8	995.5	992.1	986.6
Maximum cladding temperature, °F	1111.5	1111.6	1113.8	1121.1
Minimum cladding temperature, °F	1084.1	1084.2	1080.7	1074.4
Average pressure differential, psi	24.321	24.289	24.313	24.121
Maximum pressure differential, psi	24.352	24.399	24.332	24.223
Minimum pressure differential, psi	24.264	24.120	24.308	24.037
Δ pressure differential, psi	0.088	0.279	0.024	0.186
Δ maximum cladding temperature, °F	--	0.1	--	7.3

The appearance of the ribbed tubes currently tested at 525°C was similar to that of the tubes tested previously at 525°C, which was reported in the last quarterly report. About one-half of the rib height of some of the ribs was worn away under the dimples, and a dark oxide surface coating and some wear were apparent on all three dimples. A considerable effort was expended during this period to ensure that alignment of the apparatus and samples was good and thus was not influencing the test results. The presence of wear on all three dimples, however, indicates that some misalignment existed.

One of the tests at 525°C, which was a duplicate of previous tests, resulted in a coefficient of friction that was higher than the earlier test by a factor of 2. This higher coefficient of friction possibly indicates a sensitivity to the additional force being exerted on the ribbed tube by different dimples in the two spacers employed in each test. A cause of this problem may lie in distortion of the dimples which is a result of relaxation of residual stresses with temperature. The dimples were heavily deformed in the vicinity of the line of contact with the tube. As the two spacers are restrained by the rigid spacer holder, changes in the dimension of the dimples could change the geometry of the spacer—fuel-rod pair and thus cause additional radial force on the tube.

Tests were performed to determine the effect of high temperature on the straightness of each dimple at its line of contact and on the diameter of a ball that would contact the three dimples. Measurements of single spacer cells heated in clean helium indicate changes up to 5 mils in the dimension of the dimples. The measurements, which are made at the top, middle, and bottom of the spacer dimple, are positive in a direction normal to the axis of the spacer-grid cell. The results are

Temperature (°C)	Time (hr)	Straightness (mils)	Diameter (mils)
525	14	+3 to -1.5	+1.3 to -1.1
525	100	+2.5 to -1	+1.1 to -1.8
750	14	+5 to -2	0 to -0.2
750	100	+0.5 to -1	+0.1 to -0.4

The positive dimensions represent movement away from the axis of the cell. These changes in the extreme reduce the initial clearance between the dimples and the tube sufficiently in the case of two adjacent spacers to cause a binding or wedging action that could lead to the apparently higher coefficient of friction in the later test. The immediate solution to this problem is to remove the lower dimple, which under ideal conditions should not contact the tube. The long-range solution will be a better characterization of the spacer and improvements in spacer design and fabrication.

A series of tests were run using smooth rods to evaluate the performance resulting from impurities without the effect of rod roughening. A significant finding was the adhesion of the spacers to a smooth tube in the 525°C tests at 90 μatm H_2O and 900 μatm H_2. In one case the system was brought to temperature, stroked three times to check and adjust the alignment as necessary, and then soaked at temperature overnight. When the drive train was restarted, the spacer grid was stuck to the tube. The axial load had increased to over 15 lb, which is the overload trip for the load cells, but the spacer grid and tube were still firmly stuck. In the next test, the drive train was started immediately after the system was brought to temperature. On the initiation of the seventh 1-in. stroke, the axial load had increased to the system limit and then the system was shut down. This load is equivalent to a coefficient of friction of about 7. The spacer grid and tube were still firmly adhering at room temperature. When the spacer was removed, score marks had been produced on the tube in the area where the adhesion had occurred. The wear track was still evident on the tube and spots where metal had either transferred from the spacer or had been gouged out of the wear track were evident. Changes in the test apparatus and procedure will be made to preserve the area of adhesion in future tests so that the nature of the bond between the smooth tube and spacer can be defined better. Tests are being initiated with smooth tubes in reducing and oxidizing atmospheres to evaluate the adhesion problem in the range of 1 to 20 strokes to shed some light on the conditions that cause the adhesion and the nature of such adhesion. The lower axial blanket section of a GCFR fuel rod will be operating in the temperature range of these tests and is in the region where the greatest axial motion will occur.

The second test rig is complete and final adjustments are in progress. The 0.1-in. amplitude tests will be performed with this rig. Either test rig can be readily adapted to either stroke length or any value between 0 and about 2 in. The preliminary gas system with demountable joints has been replaced with an all-welded stainless-steel system that has demountable joints only where necessary for sensors or furnace connections. The water saturator portion of the system is all-welded copper. Additional moisture probes have been received and appear to be working well. Their performance will be confirmed when a calibration stand that is being assembled under another task is completed.

REFERENCES

1. Carslaw, H. S., and J. C. Jaeger, Conduction of Heat in Solids, 2nd ed., Oxford University Press, New York, 1959, p. 201.

2. Sinclair, E. E., "Transmittal of Meeting Report of the RRD Contractors Ad Hoc Committee on Swelling and Creep Equation Development," RRD:RT: FM-176, October 2, 1973.

3. Schroder, R. J., "Fault Trees for Reliability Analysis," USAEC, Report BNWL-SA-2522, Battelle Northwest Laboratory, February 1970.

4. McWethy, L. M., et al., "Core Design Development Needs in Relation to Fuel Failure Propagation, Sodium Boiling and Clad/Fuel-Sodium Thermal Interaction," USAEC, Report GEAP-13639-1, General Electric Co., October 1970.

5. Fontana, M. H., and MacPherson, R. E., "Work Plan for LMFBR Fuel Failure Mockup Program," USAEC, Report ORNL-TM-3902, Oak Ridge National Laboratory, April 1973.

6. "Gas-Cooled Fast Breeder Reactor Quarterly Progress Report for the Period May 1, 1973 through July 31, 1973," USAEC, Report Gulf-GA-A12728, Gulf General Atomic, October 10, 1973.

3. TASK 4120—FUEL- AND BLANKET-ELEMENT ASSEMBLIES

3.1. HEAT-TRANSFER AND FLUID-FLOW TEST

This task was initiated during the quarter with the planning of a dynamic helium loop for testing electrically heated rods that simulate GCFR fuel-rod bundles. The development of a heat-transfer and fluid-flow test facility, to be called the Core Flow Test Facility (CFTF), and the prosecution of a test program are necessary to obtain information for the design of GCFR fuel- and blanket-element assemblies. This program includes an evaluation of the operating and safety margins available during steady-state, transient, and accident conditions.

The work on this task is to be carried out under a joint program with ORNL and is to be managed by a coordinating committee that represents ORNL and GGA. At an initial planning meeting of the coordinating committee, the objectives of the program were defined, the areas of responsibility were established, and joint schedules for the overall program and for FY 74 were initiated. For the program planning document for this task, GGA will provide the following:

1. Test definition,
2. Test objective,
3. Bundle-size specification,
4. Test criteria, and
5. Instrumentation and data requirements.

The conceptual design of the facility and analysis will be provided by ORNL.

3.1.1. Test Objectives

The purpose of these out-of-pile tests is to explore a range of steady state and transient operations and a series of projected accident conditions,

including a design-basis accident. The tests will establish the design margin, safety limit, and safety margin of the element designs. This will demonstrate the ability of the fuel element, the control fuel element, and the blanket element to meet design criteria and to reduce the uncertainty in GCFR core performance.

The goal of the overall fuel- and blanket-element development program is to provide elements of each type with the structural integrity to withstand the mechanical, environmental, and thermal conditions that arise from coolant forces, differential thermal expansion, swelling of the rods due to fuel burnup, and irradiation-induced metal swelling and creep of the parts. Friction and wear of parts in sliding contact must also be considered. The overall approach to this problem involves the integration of design, analysis, and testing. The testing will demonstrate the design and verify the analysis.

The overall goal of this task is to aid in improving the performance and safety of the GCFR. The more specific goals are to provide experimental evaluation of the conceptual design of the fuel element, the control fuel element, and the blanket element and to provide experimental verification of the predictive analytical models that describe GCFR design operation and accident behavior. The generation of information on the design margin, the safety limit, and the safety margin is essential in developing the performance envelope. Since these series of tests are a bridge between the tests of specific phenomena, in-pile performance, and prototypical element behavior, the primary goal is the timely completion of these tests to confirm the phenomena tests and to reduce uncertainty in the in-pile test, in the prototypical tests, and finally in the GCFR plant operation.

The specific overall objectives of this task are to

1. Verify design analyses,
2. Establish behavior under GCFR design and off-design conditions,
3. Determine behavior during operational transients.
4. Explore GCFR depressurization accidents,

5. Test in-pile loop mockups, and

6. Explore design and safety margins.

These objectives are derived from the "Gas-Cooled Fast Breeder Reactor Demonstration Plant Development Program Plan."[1]

3.1.2. Preliminary Test Requirements

The test requirements are set by the objectives of the task. At this preliminary stage, the requirements are divided into steady-state parameters, transient rates of change for power, flow, and pressure, and extreme conditions to provide for margin testing. In addition to test conditions, the size of the test bundle is an important parameter. An average GCFR fuel element with 271 fuel rods will generate 6500 kW of thermal power. Only a portion of a GCFR element will be tested in the CFTF. Part of the initial study is to determine the cost-benefit relationship for various sizes of rod-bundle models.

The size evaluation is to determine the minimum number of rods that will effectively provide the required experimental results. In this evaluation, each type of element—fuel, control, and blanket—presents a different problem. The fuel element can be represented by a hexagonal bundle of reduced size. It must be large enough to accurately reflect edge conditions, gradients, and transient performance. An assembly with six rows of rods would have 91 rods. This is believed to be the largest practical size for testing, based on loop cost and power requirements. The control fuel element has the central 37 rods replaced by a control-rod guide tube. The control rod test bundles must simulate the effect of fuel rods located external to the guide tube. A total of 90 rods are required to provide three complete rows of rods between the guide tube and the outer wall of the element. The modeling of a complete blanket element would require 127 rods. However, since the power and flow requirements for a blanket element are small compared to a fuel element, the testing of a complete maximum-power blanket element is equivalent to a 37-rod fuel-element model that is designed for 10% overpower.

The steady-state test parameters are shown in Table 3.1 with the corresponding values for a 300-MW(e) GCFR plant. The design values for the CFTF

Table 3.1

STEADY-STATE TEST CONDITIONS FOR THE CFTF

Item	Loop Design	300-MW(e) GCFR	Remarks
Loop coolant	Helium	Helium	
Pressure, psia	1500	1310	Possible future pressure increase in GCFR
Test section			
ΔP/P test section	0.0336	0.0321	5% design margin
Inlet temperature, maximum design flow, °F	650	613	37°F design margin
Outlet temperature, nominal design flow, °F	1010	1010	
Outlet temperature, °F	1100	~1100	Out of low-power-tilt element
Coolant flow per rod			
Core, maximum, lb/hr	242	220	10% over flow in loop
Core, average, lb/hr	242	176	
Blanket, maximum, lb/hr	35	33	15% of core value
Maximum linear rating, kW/ft	16.5	15.0[a]	10% overpower
Axial maximum-to-average power ratio	1.15	1.21	
Maximum radial power gradient, $in.^{-1}$	0.10	0.065	
Total fuel rod length, in.	90	90	
Core fuel rod length, in.	40	39.2	
Axial blanket rod length (each end), in.	18	18	
Radial blanket rod length, in.	90	90	Not fueled length
Power per fuel rod,			
Maximum, kW	43	40	Includes 5% in axial blanket and 10% overpower
Nominal, kW	38	36	
Power per blanket rod, kW	11	10	15% of fuel rod

Table 3.1 (continued)

Item	Loop Design	300-MW(e) GCFR	Remarks
Nominal cold core bundle geometry			
Fuel rod OD, in.	0.25-0.30	0.282	Loop range
Pitch-to-diameter ratio	1.30-1.40	1.36	
Rod to box wall spacing, in.	0.040-0.080	0.065	Loop range
Nominal cold blanket geometry			
Blanket rod OD, in.	0.5-0.4	0.504	Loop range
Pitch-to-diameter ratio	1.15-1.25	1.20	

[a]Value for commercial GCFR plant size.

were set to allow for a small increase in steady-state values. The flow and power requirements as a function of core bundle size are given in Table 3.2.

The transient test conditions are to determine element behavior during operational and accident transients. To simulate transient operations, the transient requirements listed below are set with a margin on the rapidity of response. These are initial conceptual requirements and the feasibility and cost will be determined for the levels of transient response indicated.

Flow Transients

(100 ±1)% to (10 ±1)% in 1 sec, 2 sec, 4 sec, and 16 sec.

Continuous flow control: maximum flow to (5 ±1)%.

No specific requirements for 5% to 0% range.

Rate of change: linear within ±10%.

Other rate of change functions will be specified later.

Table 3.2

FLOW AND POWER REQUIREMENTS AS A FUNCTION OF CORE BUNDLE SIZE

Core Bundle Size (No. of Rods)	Maximum GCFR + 10% Overpower		Maximum GCFR		Average GCFR	
	Flow (lb/hr)	Power (kW)	Flow (lb/hr)	Power (kW)	Flow (lb/hr)	Power (kW)
19	4,600	820	4,200	640	3,300	490
37	9,000	1,590	8,100	1,250	6,500	960
61	14,800	2,620	13,400	2,100	10,700	1,600
91	22,000	3,900	20,000	3,100	16,000	2,400
Coolant temperature rise, °F	480		420		410	

Element Power Transients

(100 ±1)% to (10 ±1)% in 1 sec, 2 sec, 4 sec, and 16 sec.

Continuous power control: maximum power to (5 ±1)%.

Blanket element power: (20 ±1)% to 0.1%.

Rate of change: linear within ±10%.

Automatic control of element power and flow required to maintain product within ±5% of specified value.

Depressurization

Full pressure to 2 atm in 8 min, 4 min, 2 min, and 1 min.

Time tolerance: ±5%.

Final pressure tolerance: ±0.5 psia.

Rate of change to be specified later, but a flow-limiting orifice is suggested for flow control.

Element power and flow control to be coordinated with depressurizations.

Element Inlet Temperature during Transient

In the GCFR during flow-reduction transients, the reactor inlet temperature tends to decrease from 0 to 10°C. This same behavior is desired for the inlet temperature to the test element during a transient. However, this requirement may add to the cost without any significant benefit. The allowable and required inlet temperature change should initially be +10°C, 0°C, and -10°C to determine feasibility and cost. The depressurization accident causes an inlet temperature decrease of greater magnitude which can be obtained by expansion cooling in the test loop.

Slow Power Cycling of Element

To generate differential movement within a test element, a requirement for slow power cycling is specified.

Power (100 ±1)% to (10 ±1)%.

Power (10 ±1)% to (100 ±1)%.

A test may consist of 200 cycles.

For the maximum temperature requirements for margin testing of a given test element design, the coolant outlet temperature and maximum cladding temperature are a function of the power and flow. These relationships are shown in Figs. 3.1 and 3.2, where the flow is expressed as a fraction of the full power design flow and the power is expressed as a fraction of the full design power. The assumptions and method of calculation used in generating Figs. 3.1 and 3.2 are:

1. The calculations of temperature assume no change in coolant passage geometry.

2. For full power and full flow, the helium temperature rise is 400°F.

3. The temperature rise varies directly as the power fraction and inversely as the flow fraction.

4. For full power and full flow, the film temperature drop is calculated to be 158°F at the outlet where the cladding temperature is taken to be a maximum.

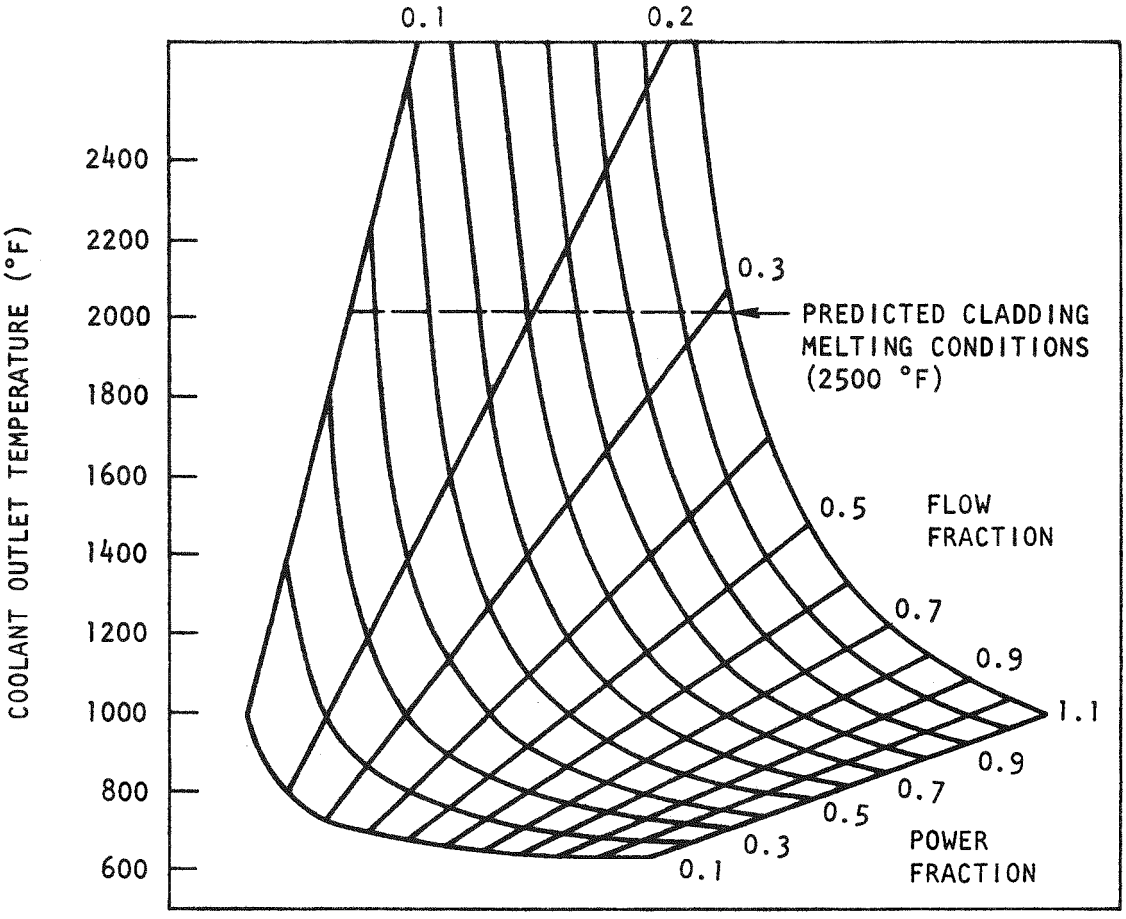

Fig. 3.1 Coolant outlet temperature

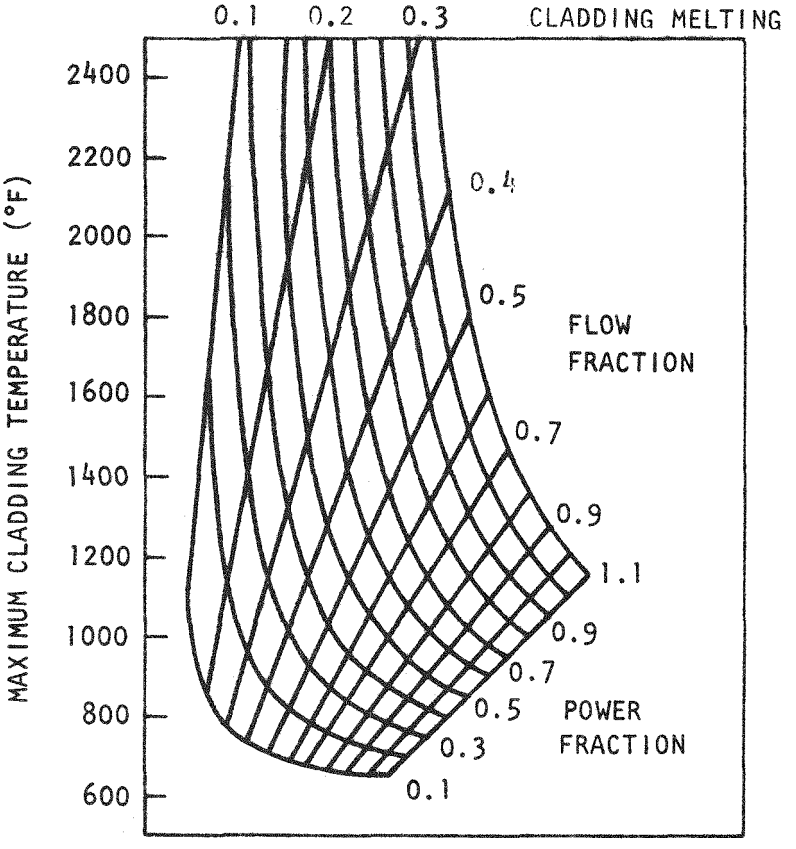

Fig. 3.2 Maximum cladding temperature

5. The film temperature drop varies directly as the power fraction and inversely as the flow fraction to the 0.94 power, allowing for the Reynolds number factor and the roughness degradation effect.

6. Inlet temperature is 600°F.

For verifying the design and safety margins by test, the plots show the operating flow and power range to obtain the over-design temperature ranges at steady state. To test at temperatures that approach cladding melting, the flow fraction must be reduced to 0.3 at full power; this condition yields an outlet temperature close to 2000°F. The achievement of these conditions in a high-pressure loop can best be realized by providing bypass cooling around the test element with dilution cooling at the outlet. The system would operate at constant flow, with the test element flow and bypass flow being adjusted to obtain the desired test element temperatures.

REFERENCE

1. "Gas-Cooled Fast Breeder Reactor Demonstration Plant Development Program Plan," USAEC, Report Gulf-GA-A10788, Gulf General Atomic, September 20, 1972, Volume II.

4. TASK 4160—PRESSURE EQUALIZATION SYSTEM FOR FUEL

4.1. ELEMENT-TO-GRID-PLATE AND VENT-CONNECTION SEAL TEST PROGRAM

In the reference design GCFR, the fuel, control, and blanket elements and their vent connections are sealed to the grid plate by clamping the matching conical surfaces of the elements and the grid plate with a force sufficient to effect a seal and to support the cantilevered elements from the grid plate. These element seals must function at the coolant pressure difference between the reactor core inlet and exit plenums. There are a number of uncertainties in the effectiveness of the seals over the life of the core because each element may be rotated or relocated several times over its useful life and because the seals must be effective in a high-purity, high-temperature helium environment and are subjected to mechanical, vibrational, thermal, and neutronic effects. Most of these uncertainties are expected to be resolved in the test programs in which materials screening for adhesion and vent-connection leakage tests will be performed. The design, procedure, and equipment for full-size element and vent-seal leakage tests will be defined and the test apparatus prepared for conducting the tests.

4.1.1. Static Adhesion Tests

The seal test program includes static adhesion screening tests of small-scale samples of conical seals that are clamped together for a period of approximately 2500 hr. The test sequence was defined and is shown schematically in Fig. 4.1. The design of the test assembly and details for this test were completed and a design review was held. The design of the test setup is shown schematically in Fig. 4.2. The screening tests will consist of the following:

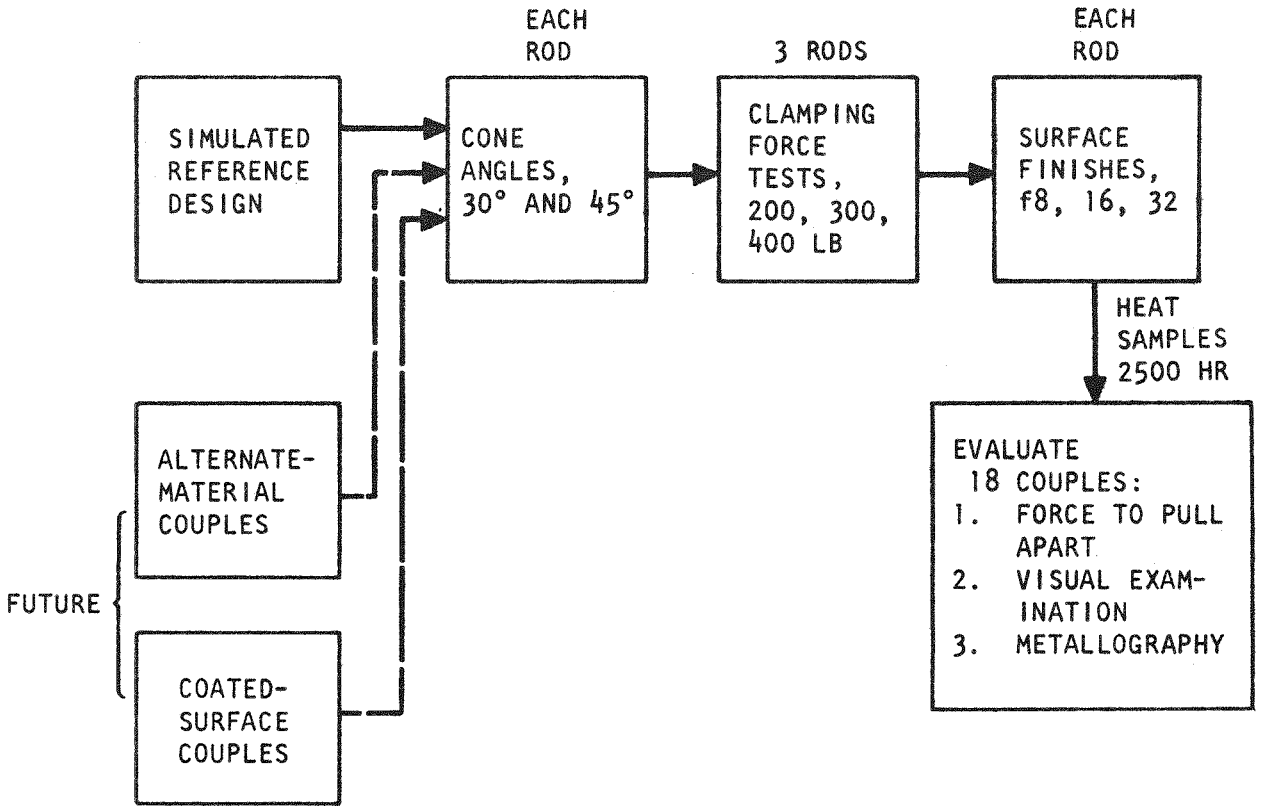

Fig. 4.1 Test sequence plan for static adhesion tests

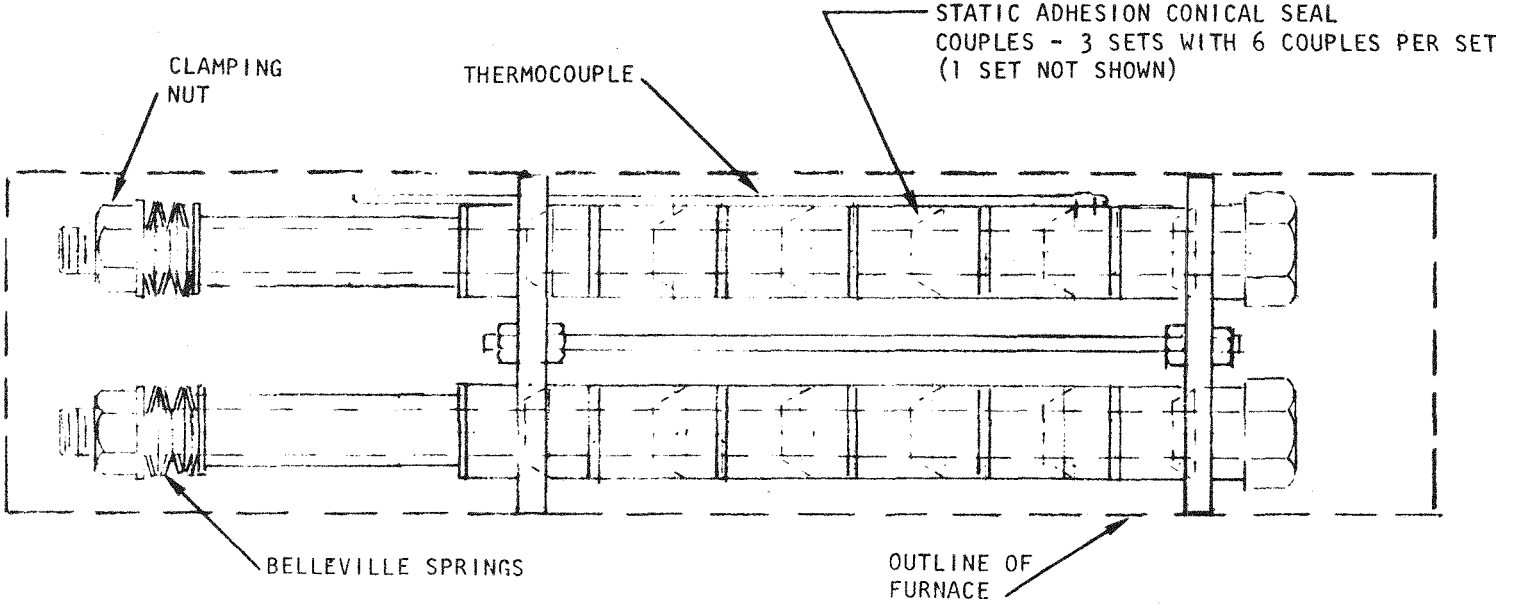

Fig. 4.2 Static adhesion test schematic

1. The first materials test will be of 18 grid-plate parts made of annealed Type 316 stainless steel clamped against an element part made of annealed Type 316 stainless steel. The 18 parts will include two cone angles, three surface roughenesses, and three clamping loads. To avoid inadvertent galling during assembly of the test couples, the conical seal parts will be keyed together to avoid a wiping motion between the sealing surfaces.

2. The second materials test will be of grid-plate parts of annealed Type 304 stainless steel clamped against an element part of Type 316 stainless steel. The number of couples will be determined from the results of the variables tested in the first test.

3. The third materials test will be of grid-plate parts of annealed Type 316 stainless steel clamped against element parts of Inconel 718. This will either be a separate test or be combined into the second test, depending on the number of test couples involved. Again, this will be determined from the results of the first test.

4.1.2. Element and Vent-Connection-Seal Leakage Tests

The major part of the seal test program is the development and performance evaluation of a full-scale conical element to grid plate seal.

The preliminary design layout and subassembly drawings for the element and vent-connection-seal leakage tests were completed. The test sequence for the seal leakage tests is shown in Fig. 4.3 and the test equipment setup is shown schematically in Fig. 4.4. The detailed design drawings for the seal leakage tests are being completed and the test plan is being prepared in final form.

4.2. MONITOR SYSTEM ANALYSIS AND INSTRUMENTATION

The purpose of this subtask is to perform research and development necessary to provide design information for a system of stations and instrumentation to monitor the activity passing through the pressure

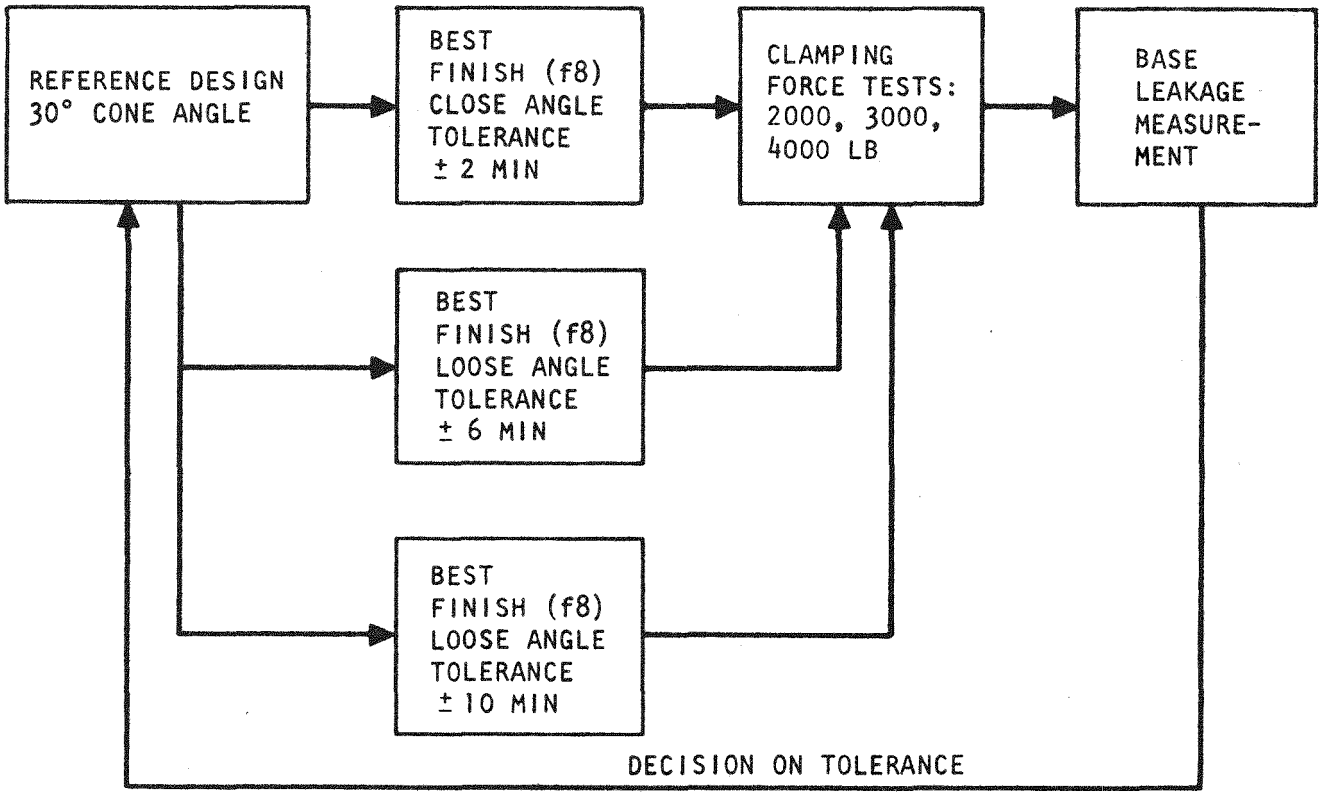

Fig. 4.3 Test plan for element and vent-connection-seal leakage tests

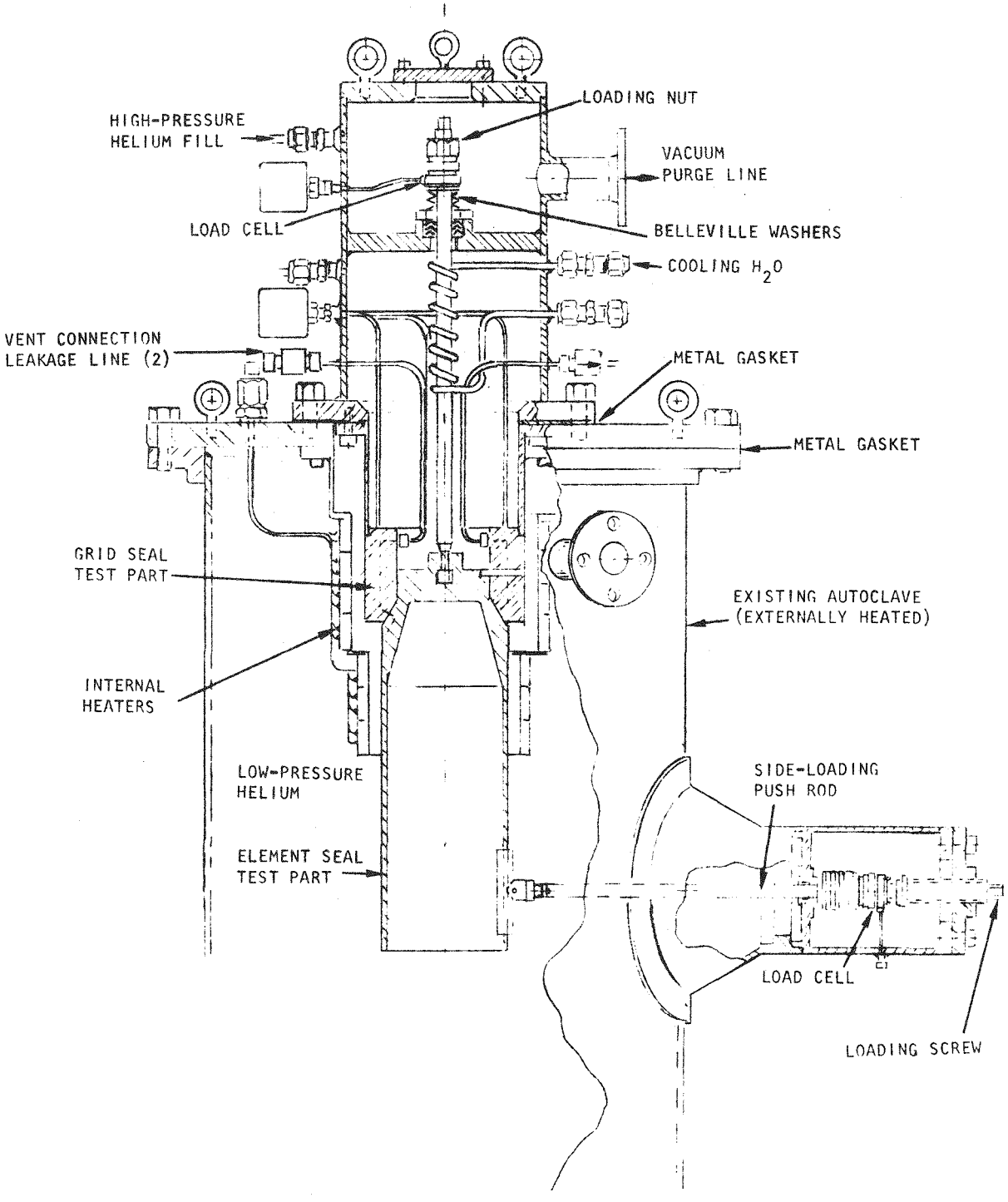

Fig. 4.4 Element and vent-connection-seal leakage test setup

equalization system from the fuel and blanket elements to the helium purification system. This monitoring system will measure activity signals resulting from leaks in the cladding of the rods in the fuel and blanket elements but will reject activity signals arising from exhalation or depressurization. Correlations of signal patterns with the location of cladding leaks and with progressive changes in the conditions of the fuel and blanket elements must be developed.

Basic information on the isotopes (fission products) in the mixtures to be expected under leaking-element conditions will be measured by a Ge(Li) analyzer system that is being prepared for installation in the gas-sampling line of irradiation capsule GB-10, which has the unique capability of simulating a leak in an operating fuel rod in an element.

The Ge(Li) analyzer system is being designed with the aid of the computer program COUNT, which is being developed as a monitor-instrumentation design tool. Options for the Ge(Li) detectors and collimators have been written into the program, as described below. COUNT can then be modified and verified by the measured data obtained for various simulated leak conditions in the GB-10 irradiation experiment.

The detailed design of the instrument mounting and gas-line configuration, assembly, calibration, and operational verification is being done by ORNL under subcontract.

4.2.1. Computer Program COUNT

Computer program COUNT computes the detector response at an activity monitoring station in the PES of a GCFR or in a sweep-gas irradiation capsule or loop. The program accounts for the release, venting, and dilution of activity from the fuel and computes the spectral response of several different detectors selected by the user's option. The program is separated into input, main body, and output sections. This arrangement is shown in Fig. 4.5, where only the main body is given in detail.

Activity birth-rate input data are obtained with the RAD-2 code.[1] The release-rate-to-birth-rate fractions are obtained with the LIFE-II code[2] using the GGA subroutine RELFRA for fission-gas release or from

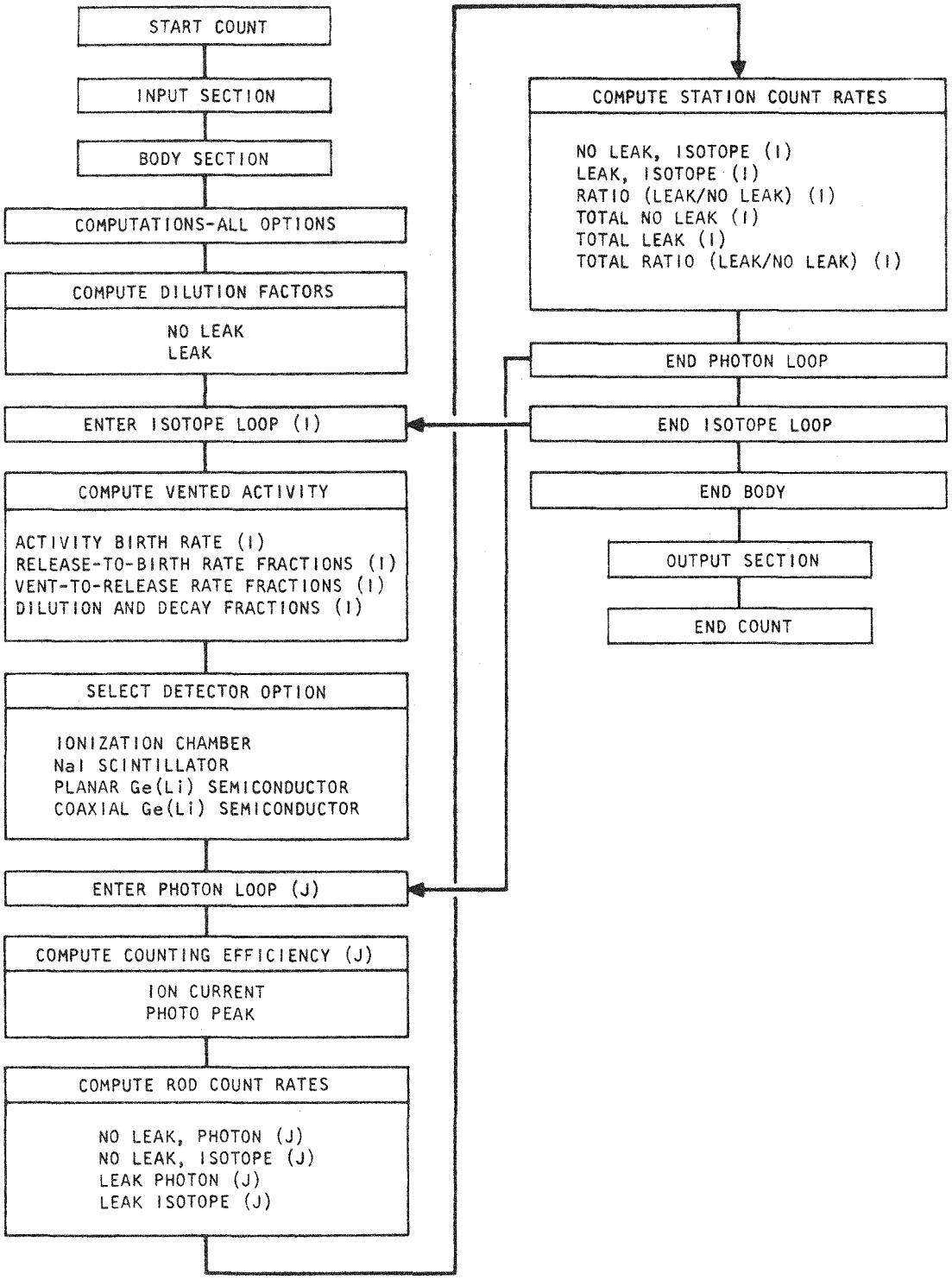

Fig. 4.5 Arrangement of input, main body, and output sections of COUNT

experiment; the venting-rate-to-release-rate fractions are obtained with the SLIDER code[3] or from experiment. The RELFRA subroutine uses coefficients of Findlay, et al.,[4] in the solid-state diffusion model.

For the installation of the Ge(Li) analyzer on the GB-10 sweep-gas line, photopeak counting efficiencies were obtained from analytical expressions found in the literature. The photopeak efficiency, η, in percent for planar Ge(Li) semiconductors[5] is given by

$$\eta = AT + B(RT^3)^{1/2} \quad ,$$

where T = thickness of detector, cm,
R = radius of detector, cm,
A = tabulated coefficient, %/cm,
B = tabulated coefficient, $\%/cm^2$.

The coefficients A and B are functions of the photon energy. Tabulated values of the coefficients A and B taken from Ref. 5 are contained in COUNT. The values used in COUNT are found by nonlinear interpolation of the tabulated values.

The relative photopeak efficiency, ε, for coaxial semiconductors[6] is given by

$$\varepsilon = 1.0 - e^{-\tau V^{1/3}} + 0.012\ V\sigma e^{-0.8E} \quad ,$$

where τ = photoelectric absorption coefficient of germanium,
σ = Compton absorption coefficient of germanium,
V = active volume of semiconductor, cm^3,
E = photon energy, MeV.

The values of τ and σ are functions of the photon energy and are taken from Ref. 7. Tables of τ and σ are program input, and the values are selected by nonlinear interpolation. The relative efficiency must then be converted to absolute efficiency of the detector, which is stated in efficiency equivalence of an NaI scintillator 3 in. in diameter by 3 in. in height to Co^{60} (E photon = 1.33 MeV) when separated from a point source by 25 cm.

4.2.2. GB-10 Sweep-gas Activity and Ge(Li) Analyzer

In the GCFR monitor system and in the GB-10 sweep-gas experiment, the concentration of activity in the flowing sweep gas is measured by the detectors. However, there is competition between the rate of dilution and the rate of decay that occurs during transit of the activity from the fuel vent to the detector. That is, although a larger sweep-gas flow rate dilutes the activity more, the activity is also carried from the fuel vent to the detector faster so that less decay occurs and thus the activity concentration is raised. Consequently, the flow rate corresponding to a maximum activity may be found as follows.

The isotopic activity concentration in the sweep gas at the analyzer is given by

$$A_i = \frac{C_i}{Q} e^{-\lambda_i t} \quad ,$$

where A_i = activity concentration in the sweep gas, Ci/cm^3,
C_i = venting or release rate, Ci/sec,
Q = leak or dilution rate, cm^3/sec,
λ_i = decay constant, sec^{-1},
t = transport time, sec,
V = volume of the sweep line between the fuel vent and detector, cm^3,

and the subscript i denotes the i^{th} isotope in the gas.

Since

$$t = V/Q,$$

$$A_i = \frac{C_i}{Q} e^{-\lambda_i V/Q} = f(Q) \quad .$$

The activity concentration will be maximum where its rate of change with respect to the flow rate is zero. Evaluating the maximum activity concentration, we have at $A_{i(max)}$

$$\frac{dA_i}{dQ} = \frac{C_i}{Q^2} e^{-\lambda_i V/Q} \left(\frac{\lambda_i V}{Q} - 1 \right) = 0 \quad ;$$

therefore

$$Q(A_{i(max)}) = \lambda_i V = QMAX \quad .$$

The total activity is

$$A = \sum_{i=1}^{N} A_i \quad .$$

The maximum activity concentration of each isotope occurs at a different flow rate. Thus, the relative concentration of isotopes in the gas mixture will be different for each flow rate. Since the QMAX values are well separated, by orders of magnitude in most cases, measurement of A versus Q will indicate the predominate activity present in each case. Also, to measure the activity levels present, the flow rate may be adjusted to maximize the isotope of interest. At the present GB-10 sampling rate, Kr^{89} is favored. For longer-lived isotopes, smaller flow rates are more favorable and vice versa. The COUNT program indicates that at normal purge rates, Xe^{138} predominates for capsule GB-10 in the flow mode in through the bottom of the fuel and out through the top of the trap, whereas Xe^{135} predominates for the flow mode in through the top of the trap and out through the top of the trap. Typical results are shown graphically in Fig. 4.6 for the "no-leak" simulation flow mode (i.e., sweeping across the top of the trap) and in Fig. 4.7 for the "leak" simulation flow mode (i.e., sweeping through the fuel, blanket, and trap). The design must result in adequate counting rates for both flow modes without saturating the detector. This is being parametrically studied with variables of collimator size, separation distance, sample-line size, and gas flow rates. Further information is given below.

4.2.3. Ge(Li) Analyzer Installation

A subcontract has been arranged with ORNL for completion of the detailed design, installation, calibration, and operational verification of the Ge(Li) analyzer system.

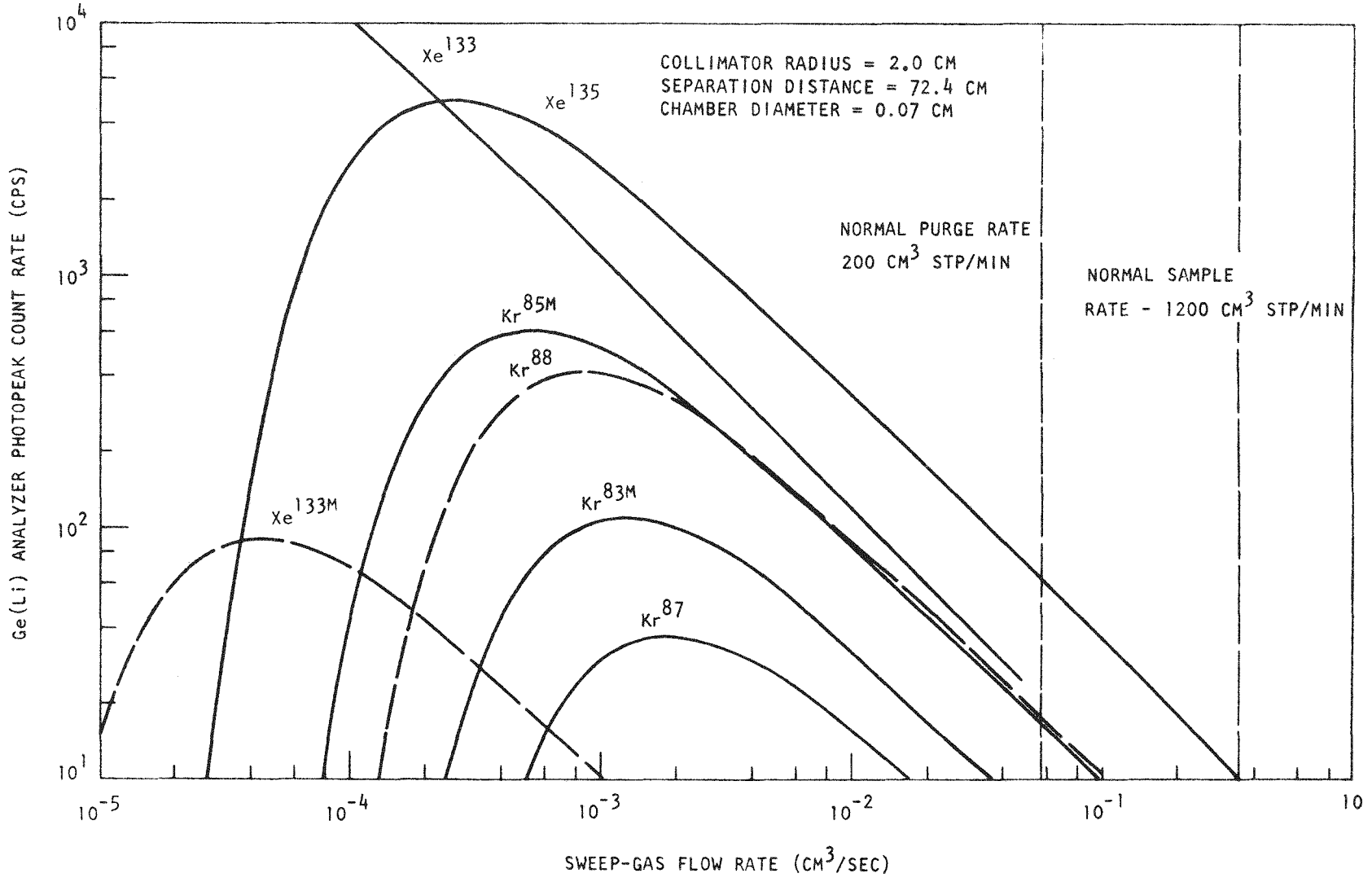

Fig. 4.6 Sweep-gas flow rate (actual cm^3/sec) for flow in through the top of the trap and out through the top of the trap in capsule GB-10

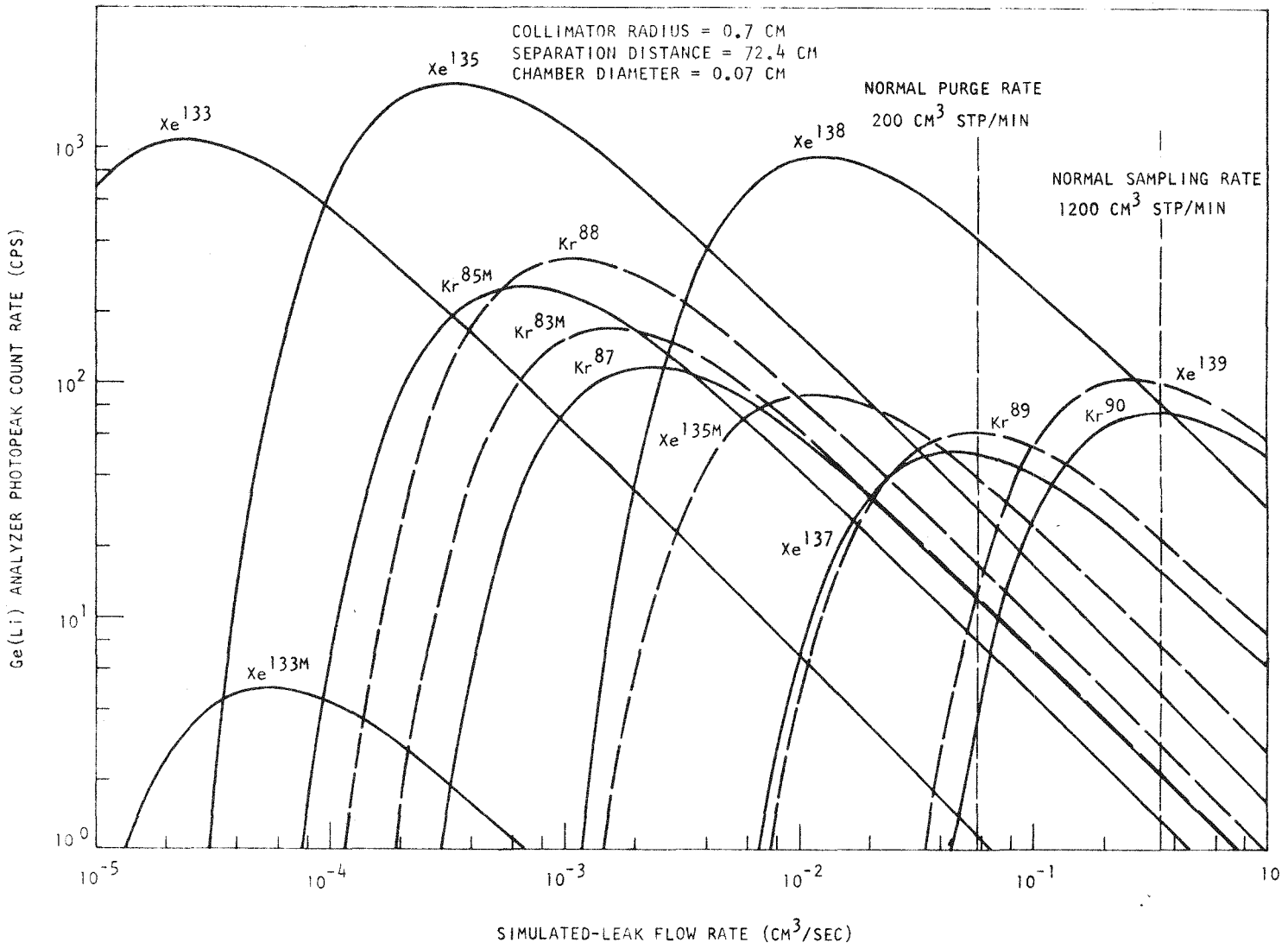

Fig. 4.7 Simulated-leak flow rate (actual cm^3/sec) for flow in through the bottom of the fuel and out through the top of the trap in capsule GB-10

Considerable progress has been made in defining the equipment, location, and configuration of the Ge(Li) analyzer at the ORR by GGA and ORNL. The original concept was to hang the detector over the side of the ORR pool and insert collimator pipes into the water to "look at" the sample-gas lines. This was found to involve unsatisfactory operational aspects, such as equipment falling or being knocked into the pool and high moisture levels in the electronic equipment. Space around the GB-10 shielded valve box was too congested, and the minimum line-to-detector separation distance was found to be undesirably large (28 in.). Thus, a small-diameter bypass line will be ducted to an adjacent cell in the ORR building where the detector will be located. This will allow greater flexibility in the choice of separation distance and in collimator opening size and thickness. Valving for the bypass loop will be installed in the GB-10 shielded valve box.

To avoid a procurement delay of approximately three months, a Ge(Li) detector that meets the requirements of the analyzer system is to be loaned by GGA to ORNL for the duration of this program. The detector description is given below.

Princeton Gamma Tech Ge(Li) Coaxial Detector
Serial No. 509
Efficiency 8.6%
Resolution 2.3 keV (FWHM)
4.2 keV (FW.1M) } at 1.33 MeV
Peak/Compton Ratio 24:1
Nominal Active Volume 45 cm^3

Since the GGA detector is vertically mounted, alteration to horizontal mounting was anticipated. However, subsequent consideration indicated that the loss of efficiency by photons entering the side of the detector housing where the aluminum walls are thicker than the end window would be trivial compared to the loss from the stainless-steel gas-sampling line.

Data-taking and -processing equipment for the Ge(Li) analyses at ORNL and GGA were found to be incompatible. Significant additional effort and

cost at ORNL will be required to program and operate data conversion equipment to make the data analyzable on GGA equipment. For this reason ORNL will reduce the spectral data and will transmit the results to GGA.

4.3. FISSION-PRODUCT-MANIFOLD FABRICATION DEVELOPMENT

In the reference GCFR design, a manifold is employed to interconnect the interior of the rods of each fuel element and blanket element to equalize the pressure inside and outside the fuel-rod cladding and to permit venting of the fission gases. The manifold also serves as a support grid for the fuel rods. The purpose of this task is to develop means for fabricating and testing a manifold for the GCFR fuel rods that will function reliably throughout the design life of the fuel element. This would will include the development of a satisfactory means for connecting the fuel rods to the manifold and connecting the manifold to the fuel-element trap. The chosen fabrication methods must be adaptable to adequate quality control inspection and to meet practical scale-up requirements for economic large-scale production. Environmental effects on the stability and life of the manifold will be evaluated. The adequacy of the manifold design for precluding fission-product plugging will be determined.

Several different conceptual designs will be evaluated for performance, fabricability, adaptability for adequate quality control inspection, and effect of geometry on coolant pressure drop. A preferred design will then be chosen. The processes for fabricating the preferred design manifolds, drilling holes into the manifolds, and joining the manifold to the rods and element trap will then be evaluated to determine which methods show the most promise for control of tolerances, economy, and utility.

During this quarterly period, work on the development of the fission-product manifold consisted of (1) documentation of the design criteria for the fission-product manifold, (2) completion of a plastic model of a two-level manifold concept, (3) preparation of a test plan and procedures for testing the metal-to-metal seals that are proposed to be used to join the fuel rods and the tubes connecting the element trap to the manifold, and (4) fabrication of test samples of the rod seal.

4.3.1. Design Criteria

A design criteria document for the fission-product manifold has been prepared. The criteria cover materials and structural and pressure-equalization-system functions.

4.3.2. Plastic Model

In the reference GCFR fuel-element design, a single-level manifold is used, such as the one shown schematically in Fig. 4.8. A two-level concept such as that shown schematically in Fig. 4.9 has been suggested to reduce the pressure loss in the coolant flowing over the structure and to provide more space between the fuel and blanket rods for attaching the rods to the manifold. Rows of rods are attached alternately to the upper and lower levels. Separate subassemblies attaching the rods to the upper and lower levels would be fabricated and leak checked and then the two subassemblies would be assembled. Fabrication of a plastic model of the two-level concept has been completed (see Fig. 4.10). The model was used to evaluate the adequacy of the space between the rods for heliarc welding of the rods to the manifold using conventional equipment. The model indicated that this two-level design did not provide adequate welding space, but it appears to be adaptable to a screwed metal-to-metal connection of the rods to the manifold.

4.3.3. Test Plan

The draft of the test plan and procedure for testing the screwed metal-to-metal seals of fuel rods to the manifold is being revised. The revision reflects the fact that a decision was made that the tests during the current fiscal year would involve screening seven different types of seals rather than performing more elaborate tests on two candidate seals as originally planned.

4.3.4. Screwed-rod Connection Samples

Samples have been prepared for evaluation of metal-to-metal threaded joints used to effect a seal between the fuel rods and the fission-product manifold. The experimental arrangement that will be used for measuring

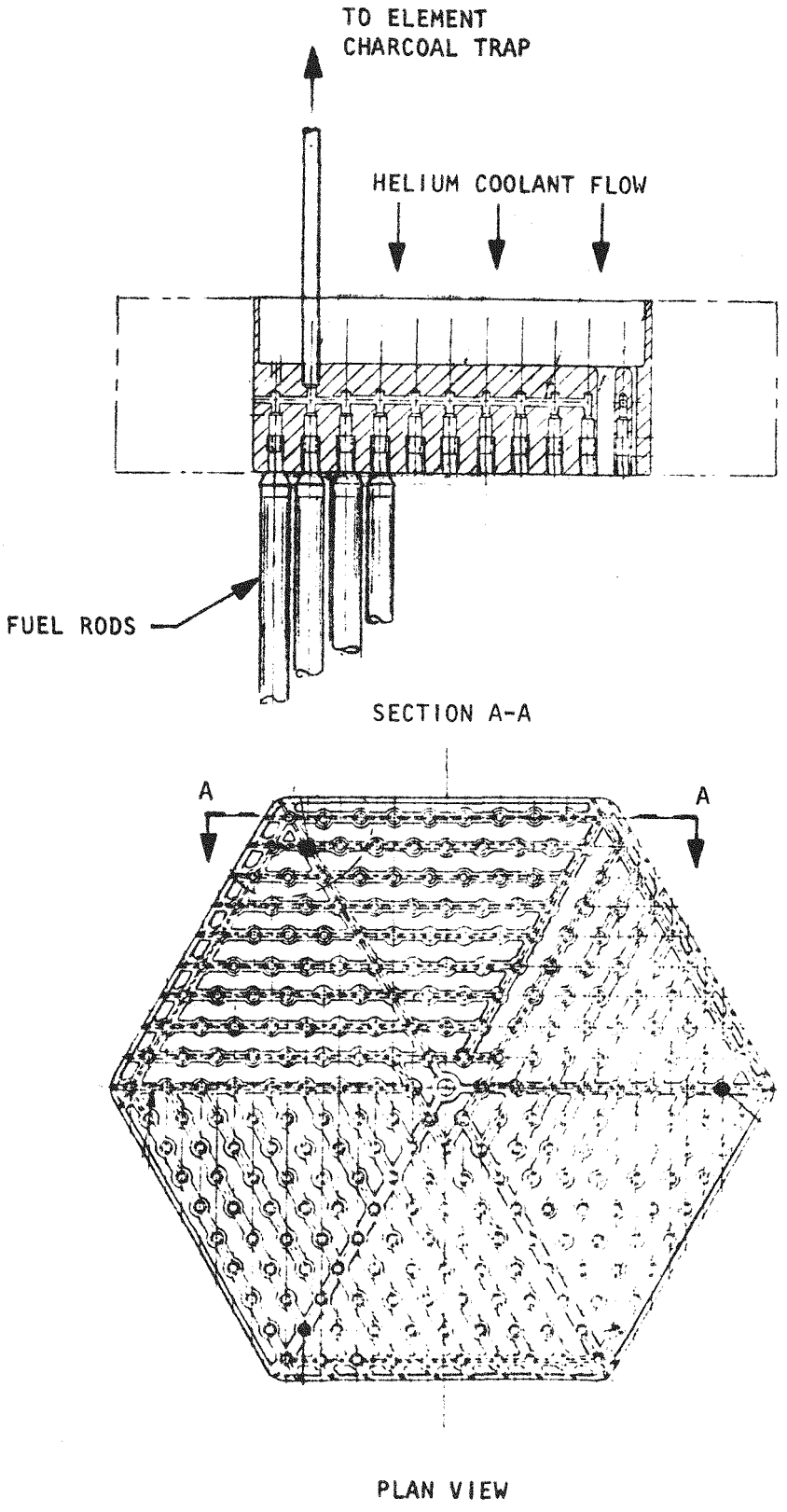

Fig. 4.8 Single-level fission-product manifold schematic

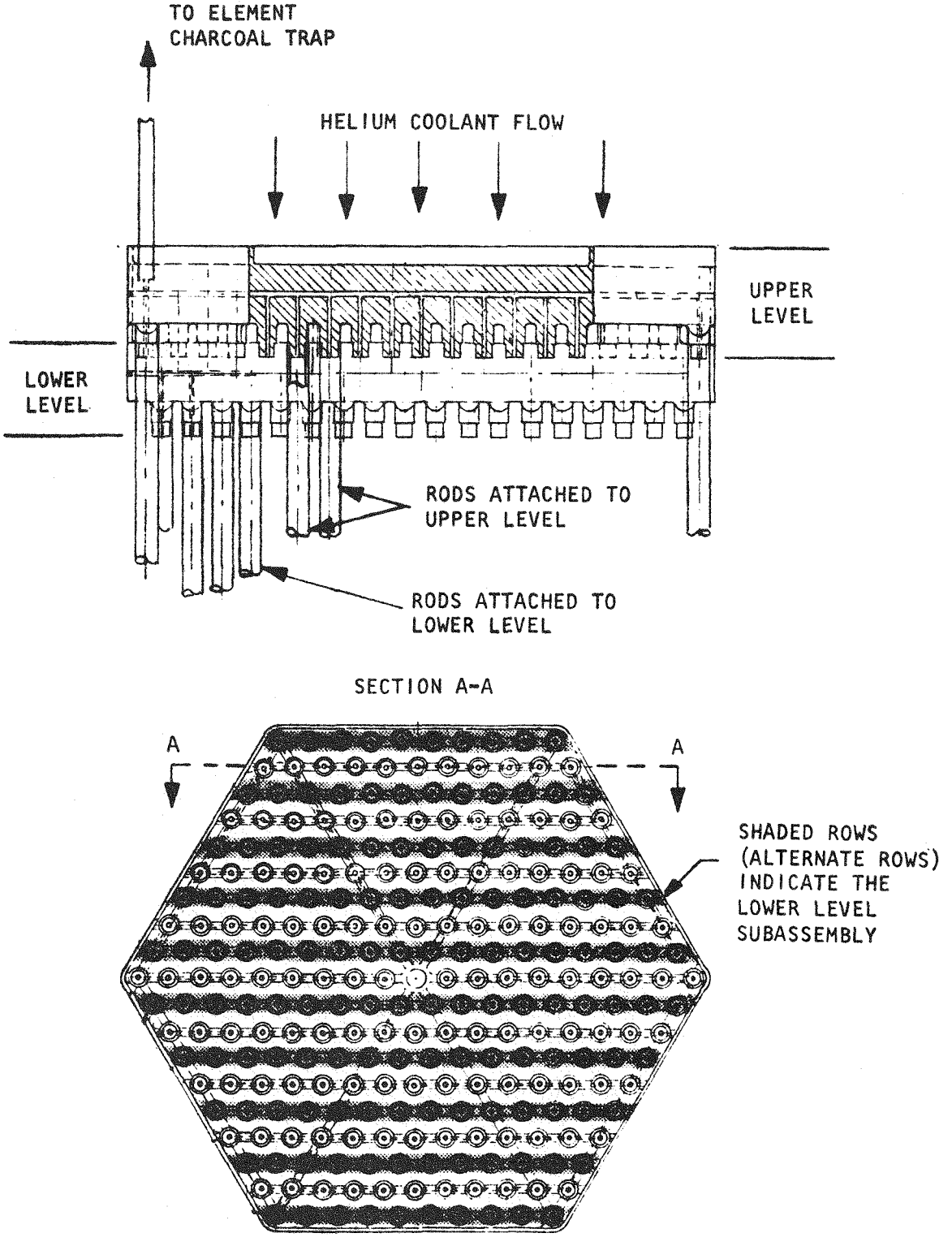

Fig. 4.9 Two-level fission-product manifold schematic

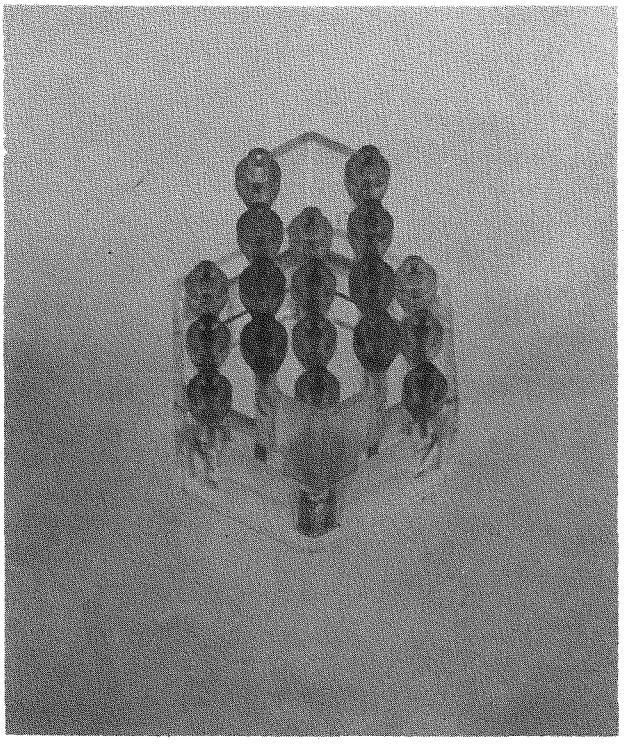

Fig. 4.10 Two-level fission-product manifold model

the leak rates of the various seal designs is shown in Fig. 4.11 and a photograph of the test fixture and typical seal gaskets is shown in Fig. 4.12. The types of seals to be evaluated are listed below.

1. Lock Ring Seal - A tube that is slightly bell-shaped at one end is slipped over a straight tube and then a lock ring tapered inside is slipped over the mating section to elastically deform both tubes and create the seal. (This type of seal has been successfully developed for a number of aerospace and domestic applications including the B-1 bomber for NASA.)

2. "K" Seal Plated - A modified "U" seal with outward curving legs that touch both sealing surfaces; the "U" is elastically deformed with a low applied force to effect the seal.

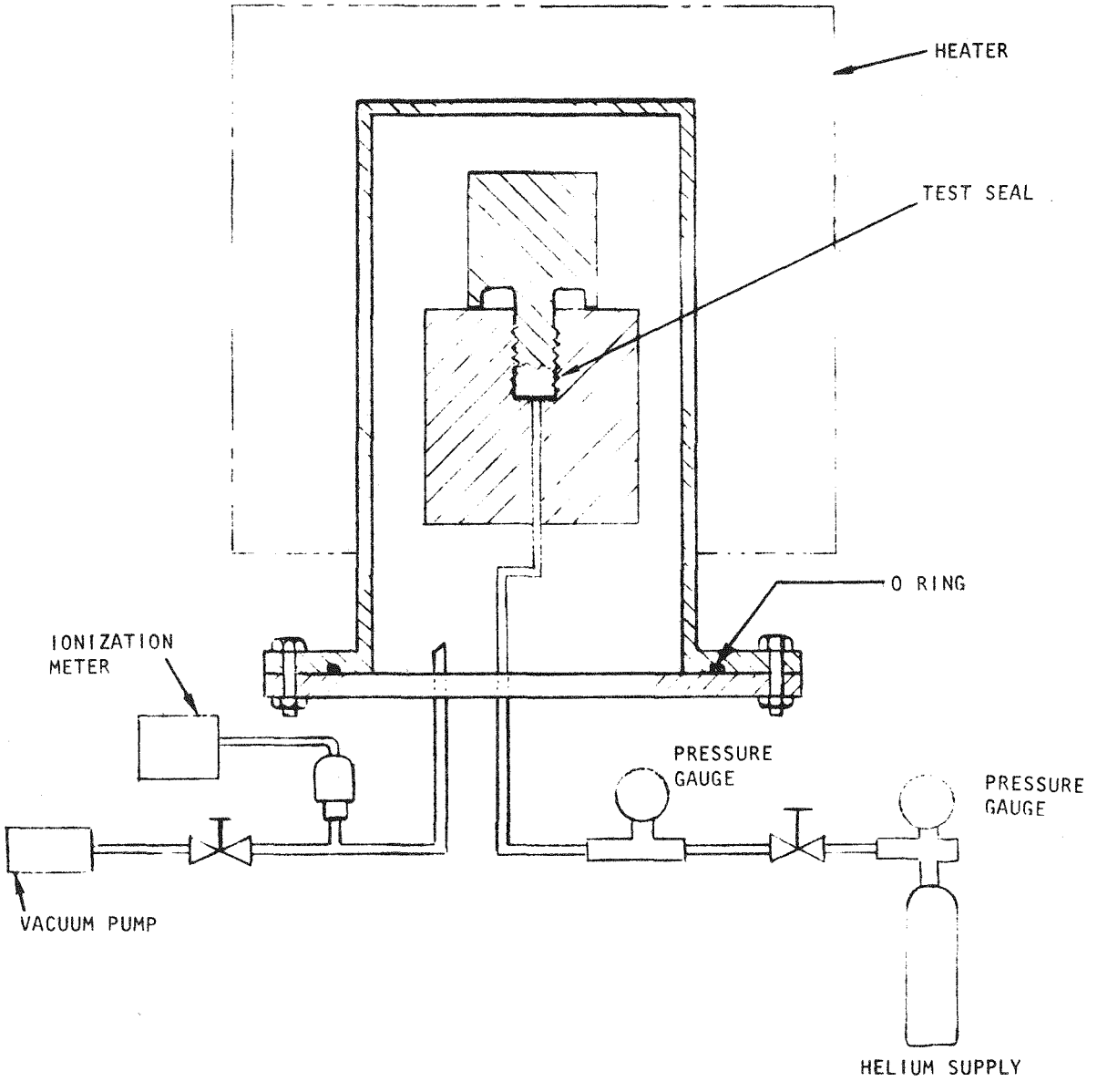

Fig. 4.11 Schematic of arrangement for leak-testing metal-to-metal threaded connectors

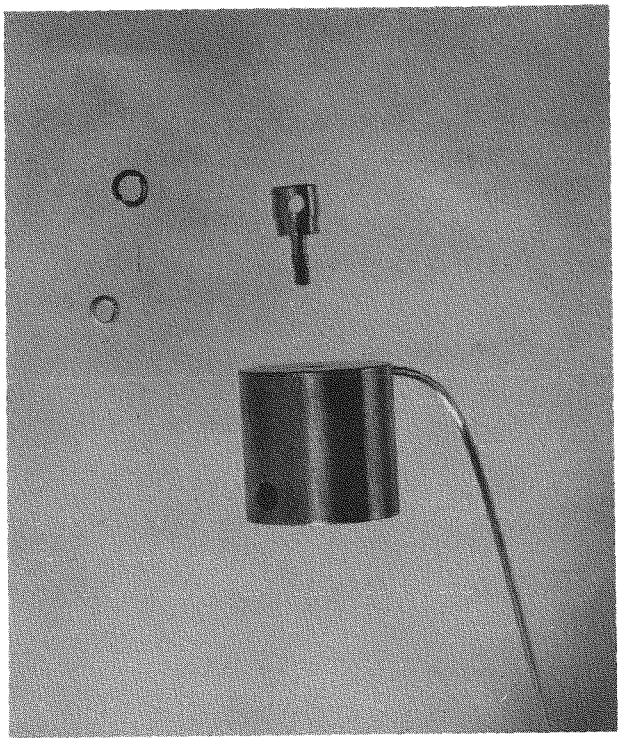

Fig. 4.12 Samples of metal-to-metal threaded connectors for screening leakage tests

The design allows flexing of the seal after the initial joint is made. The addition of plating allows a more plastic sealing surface which does not impose stringent requirements on the finish of mating surfaces.

3. "K" Seal Unplated - Identical to item 2, above, without plating. The sealing surface must be of a finer finish to effect sealing.

4. "V" Seal Plated - A "V" seal with legs touching both mating surfaces. The "V" is elastically deformed to create the seal. The plating allows a more plastic sealing surface.

5. Flat Bottom Seal - A threaded tube is inserted into a cup and the mating surfaces effect a seal.

6. Sparkplug Type of Cone Seal - Two cone-shaped surfaces with slightly different cone angles. When one cone is inserted into the

other, plastic deformation of the cone surfaces occurs to create the seal.

7. Sparkplug Type of Gasket Seal - A flat gasket of copper is inserted between the two sealing surfaces. Applied pressure causes the plastic deformation of the gasket to create the seal.

REFERENCES

1. Vanslager, F. W., "RAD-2, A computer Program for Calculating Fission Product Radioactivities," USAEC, Report GAMD-6519, General Dynamics Corporation, General Atomic Division, July 23, 1965.

2. Jankus, V. Z., and R. W. Weeks, "LIFE-II, A computer Analysis of Fast-reactor Fuel-element Behavior as a Function of Reactor Operating History," Nucl. Eng. Design, Vol. 18, No. 1, 1972, pp. 83-96.

3. Jadhov, K. B., and B. W. Roos, "SLIDER, A Fortran V Program for the Computation of the Release of Fission Products from One-dimensional Multilayered Fuel Configurations," USAEC, Report GA-8566, Gulf General Atomic, August 1, 1969.

4. Findlay, J. R., et al., "The Emission of Fission Products from Uranium-Plutonium Dioxide during Irradiation to High Burnup," J. Nucl. Mat., Vol. 35, 1970, pp. 24-34.

5. Harvey, J. R., "A Formula for Predicting the Sensitivity of Ge(li) Spectrometers to Gamma Rays in the Range 0.4 - 1.5 MeV," Nucl.Instr. Methods, Vol. 86, 1970, pp. 189-197.

6. Paradellis, T. and S. Hontzeas, "A Semiempirical Equation for Ge(Li) Detectors," Nucl. Instr. Methods, Vol. 73, 1969, pp. 210-214.

7. Freeman, J. M., and J. G. Jenkins, "The Accurate Measurement of the Relative Efficiency of Ge(Li) Gamma-ray Detectors in the Energy Range 500 to 1500 keV," Nucl. Instr. Methods, Vol. 43, 1966, pp. 267 - 277.

5. TASK 4200/4400—FUELS AND MATERIALS DEVELOPMENT

5.1. THERMAL-FLUX IRRADIATION EXPERIMENTS

5.1.1. Irradiation Capsule GB-9

The shipment of irradiated materials containing the charcoal trap, cladding specimens, and dosimetry monitors from irradiation experiment GB-9 was received at the GGA Hot Cell Facility and postirradiation examination is under way on the charcoal trap.

After the charcoal trap, cladding specimens, and dosimetry bandoliers were removed from the shipping container, the cladding and dosimetry samples were monitored for gross activity levels and then placed in storage containers in the high-level hot cell. The cladding specimens will be used for confirming the Kr^{85} annealing technique to be used for determining the cladding operating (irradiation) temperature of fuel rods in noninstrumented capsules such as those in the fast flux F-1 (X094A) irradiation experiment. The dosimetry specimens will be retained in storage until the required analysis can be performed.

The charcoal trap was gamma-scanned for fission-product activity. Neither Cs^{134} nor Cs^{137} were detected at above background levels using a NaI detector. This finding suggested that the activity on the charcoal was low and that the principal contributor to the activity was activation of the stainless steel of the trap. Before it was disassembled, the charcoal trap was monitored in-cell and the reading was 250 R/hr at 6 in. Essentially all of this activity was due to activation of the stainless steel since the individual charcoal samples read only ~300 mR/hr at 2 in.

An axial slit was made along the entire length of the GB-9 charcoal trap with a 0.05-in. abrasive wheel. The slit proved to be adequately wide to permit removal of all of the charcoal. (Unfortunately, the high

rotational speed of the wheel ejected some of the charcoal from the trap during the slitting operation so that some of the charcoal was lost.) The trap was then transferred to a fixture designed to divide the charcoal sample into six axial fractions without contaminating the sample containers. Precautions against contamination of the sample containers were taken to ensure that the samples could be removed from the hot cell and brought to the analytical laboratories provided that the activity on the charcoal was indeed low. Sixty-seven percent of the charcoal in the trap was recovered in the axially sectioned fractions and when the ejected material was collected, a total of 82% was recovered.

The axially sectioned charcoal samples were brought to the GGA Gamma-spectrometry Facility for analysis on a Ge(Li) detector. Very low levels of Cs^{137} and Cs^{134} were detected in each fraction except in the fraction that was farthest from the fuel. The Cs^{134} profile was essentially flat in the first four fractions, but both cesium loadings may have decreased slightly in the two fractions farthest from the fuel.

The samples were given preliminary examinations by X-ray spectroscopy and cesium and iodine were detected. Tellurium was not detected, possibly because of X-ray line interferences. As the cesium loading determined by X-ray spectroscopy appeared to be about an order of magnitude higher than the loading determined by gamma spectrometry and fission yields, this analytical procedure was not continued.

Isotopic iodine analyses are being carried out by neutron activation analysis on several of the samples. The I^{129} loadings are in the range of 2.5 to 6.1 μg/g of charcoal with no statistically significant axial gradient. Since the I^{127} fission yield is only ~10% of the I^{129} yield, these values essentially represent the total iodine loading of the charcoal.

Isotopic cesium analyses of samples of three axial fractions were made by mass spectrometry. The average values of two determinations on each sample are given in Table 5.1. It should be noted that Cs^{134} is not a fission product since it has no direct fission yield and its Xe^{134} precursor is a stable isotope. However, Cs^{134} does result from an (n, γ) reaction

Table 5.1

CESIUM ISOTOPIC ANALYSIS OF GB-9 CHARCOAL TRAP SECTIONS

(In atom-%)

Trap Location	Sample Number	Cs^{133}	Cs^{134}	Cs^{135}	Cs^{137}
Inlet	965	48.7	0.4	49.7	1.2
Middle	964	47.8	0.4	50.4	1.4
Outlet	963	46.8	0.4	51.1	1.7

on the fission product Cs^{133}. Thus, the quantity of Cs^{134} in the charcoal trap is produced from Cs^{133} released from the fuel. In evaluating the fractional releases of each mass chain, the Cs^{134} assay should be added to the Cs^{133} assay. The resulting isotopic fractions are listed in Table 5.2. These data have not yet been subjected to detailed analysis. However, even though the fission yields of the three mass chains are roughly equal, it is evident from these tables that the fractional releases of Cs^{133} and Cs^{135} from the fuel and blanket regions are much higher than the fractional release of Cs^{137}.

Table 5.2

ISOTOPIC ANALYSIS OF GB-9 CHARCOAL TRAP SECTIONS[a]

(In atom-%)

Trap Location	Sample Number	Cs^{133}	Cs^{135}	Cs^{137}
Inlet	965	49.1	49.7	1.2
Middle	964	48.2	50.4	1.4
Outlet	963	47.2	51.1	1.7

[a]Based on released mass chain.

The three cesium isotopes in Table 5.2 are either stable or their half-lives are long (compared to the migration time). Therefore, the differences in fractional release cannot be accounted for by migration of cesium. The

xenon precursors Xe^{135} ($T_{1/2}$ = 4.2 h)* and Xe^{133} ($T_{1/2}$ = 5.3 d) apparently have lifetimes long enough to permit roughly equal release fractions. Additional analysis will be required to quantitatively assess the migration phenomena.

Charcoal samples are also being leached for extraction of strontium so that isotopic assay for Sr^{89} and Sr^{90} may be carried out by beta counting. This analysis will yield data on the migration of the lighter fission-product fractions due to the strontium precursors krypton and rubidium.

5.1.2. Irradiation Capsule GB-10

The vented-fuel-rod sweep-gas capsule experiment GB-10 had reached a burnup of 29,700 MWd/Te in the ORR at the end of this reporting period.

Irradiation of capsule GB-10 resumed after the scheduled maintenance shutdown of the ORR in August and the capsule was operated at 12 kW/ft and a cladding outer surface temperature of 565°C until equilibrium conditions were reestablished. After a burnup of ~27,000 MWd/Te, the power was then increased to 13.5 kW/ft. Increasing the power level from 12 kW/ft to 13.5 kW/ft resulted in an increase in the activity in the fission-gas monitor line by a factor of 6, which was expected.

On October 12, 1973, a leak in the sweep-gas line of the GB-10 experiment was discovered and the GB-10 capsule assembly was retracted from the ORR. Prior to the occurrence of the valve leak, capsule GB-10 had accumulated ~2,700 MWd/Te while operating at the 13.5 kW/ft power level. When irradiation is resumed capsule GB-10 will continue to operate at the 13.5 kW/ft power level until steady-state fission-gas release conditions are attained or until the limitation of burnup requires going to 14.8 kW/ft, at a cladding temperature of 685°C, to obtain high priority data.

Before the power of capsule GB-10 was raised to 13.5 kW/ft, two neutron radiographs were taken of the fuel rod at the same angle but at different exposures to maximize information in the fuel and near the bottom of the upper blanket where the sweep-gas line terminates. The radiographs reveal

*The true half-life of Xe^{135} is 9.2 h, but its effective half-life in the ORR core is ~4.2 h as a consequence of its 2.6×10^6 barn cross section.

nothing about the sweep-gas line and fission-product deposition in that region. In agreement with LIFE-II predictions, a central hole had not been formed in the fuel region, although there may be a trace of one starting near the top of the fuel stack. The radiographs showed some filling of the end dishes in the pellets but individual pellets were easily discernible. In agreement with expectations for the low density fuel (88% TD), overall shrinkage of the fuel column was apparent by two interpellet gaps. One gap between the top mixed-oxide pellet and the adjacent enriched UO_2 half pellet was ~1/16 in. and the other gap between the first and second upper blanket pellets was ~7/64 in. In addition to these gaps (i.e., including the pellet to pellet gaps), the fuel and blanket column shortened ~3/32 in. No radial shrinkage was apparent—the fuel and cladding appeared to be in good contact.

Also prior to raising the capsule power to 13.5 kW/ft, the pressure drop of the sweep gas flowing through the fuel rod (in through the bottom of the fuel rod and out through the top of the trap) had risen to 35 psi at the standard sampling flow rate (~1200 cm^3 STP/min). Except during initial startup, the pressure drop for these conditions had been stable at ~15 psi. When the power level was increased from 12 kW/ft to 13 kW/ft, a pressure-loss transient up to 60 psi and back to ~35 psi occurred in the 24-hr period following the increase in power. A week later the pressure-loss was stable at the 35-psi level. The reasons for the pressure-drop changes are not known.

During the ORR refueling shutdown in October, lowering the pool water level exposed the sampling and sweep-gas lines mounted on the side wall of the pool and presented an opportunity to measure fission-product deposition in the lines. The dose rates measured by ORNL two days after shutdown were reported to be

Near the capsule lines to the shielded valve box (mounted on the outside of the pool wall)	0.7 R/hr
Downstream of junction box (along pool wall)	7 R/hr
Upstream of junction box (where lines leave the wall and enter the lowered level of water)	10 R/hr

Just prior to shutdown of the ORR and lowering of the pool water, gas samples were taken using the flow modes in through the bottom of the fuel and out through the top of the trap (BF-TT) and in through the top of the trap and out through the bottom of the blanket (TT-BB). Constriction of flow in the exit line from the fuel-blanket interface, i.e., flow modes that exit through the bottom of the blanket (XX-BB), has previously been observed in capsule GB-10, especially during the flow mode in through the bottom of the fuel and out through the bottom of the blanket (BF-BB). Furthermore, experience with vented capsule GB-9 and with the first eight capsules of the fast flux F-1 series indicated that cesium and iodine accumulated at the fuel-blanket interface. It is thus presumed that operation of capsule GB-10 in the TT-BB flow mode transported some radioactive cesium and iodine into the exit line. If our presumption is correct, the deposition is a characteristic of the irradiation experiment and not a condition to be expected in a GCFR where normal flow in leaking rods can only exit from the top of the rod traps. ORNL is planning to make spectral measurements of the activity to identify the fission products in the lines and their relative amounts.

5.2. FAST-FLUX IRRADIATION EXPERIMENTS

5.2.1. Fast-flux Irradiation Experiment F-1 (XO94A)

The second interim examination was completed on the seven encapsulated fuel rods (G-1, G-2, G-4, G-5, G-6, G-7, and G-8) after burnup exposures up to 56,000 MWd/Te were reached in the initial six fuel rods. (Capsule G-3 was replaced with capsule G-8 during the first interim examination.)

The five fuel-rod capsules that were removed from the subassembly (G-1, G-2, G-5, G-6, and G-7) were sent to ANL-East for destructive examination. Those were replaced with five unirradiated encapsulated fuel rods. The F-1 (XO94B) subassembly has been reconstituted and is ready for reinsertion in EBR-II for Run 67 (which is scheduled to occur in early November).

Upon reinsertion of the F-1 experiment in EBR-II, irradiation of the seven-rod subassembly will continue to a burnup goal of 100,000 MWd/Te on the remaining initial fuel rod (G-4).

Neutron radiography of the fuel rod capsules during the second interim examination showed no unusual features except that there was approximately 50 vol-% shrinkage of the activated charcoal in the fuel rods traps due to the fast neutron fluence. Some charcoal shrinkage is also expected in the 300-MW(e) GCFR but the design fast fluence to the charcoal traps has decreased primarily because of the addition of neutron shielding in the GCFR fuel rods. The neutron spectrum has also been shifted. Preliminary calculations indicate that the maximum fast fluences to the charcoal traps in the F-1 experiment now exceed the design values for the 300-MW(e) plant. Both the 300-MW(e) GCFR fluence and the EBR-II fluence are being reevaluated.

Analysis of the data obtained during both the initial gamma scanning in March 1973 and the supplemental scanning in August 1973 continued at GGA.

Analysis of the diametral scans of rods G-1, G-4, and G-8 taken during the initial phase of the second interim examination in March 1973 has been completed. A typical diametral fission-product profile for a nonvolatile species (Zr^{95}) is shown in Fig. 5.1. In contrast, volatile species exhibit peaking at the fuel-blanket interface, which confirms the results reported during the first interim examination at 25,000 MWd/Te.[1] Data obtained during the 50,000 MWd/Te examination for I^{131} and Cs^{137} in rod G-1 are plotted in Figs. 5.2 and 5.3. The data shown in Figs. 5.1 through 5.3 were obtained in the fuel region just below the upper fuel-blanket interface. Similar diametral profiles are also seen in the blanket region.

The diametral distribution of Mn^{54} has been used to determine the diameter of maximum activity of the three concentric tubes of the F-1 capsules. The experimental values are compared with the calculated values in Table 5.3 for fuel rods G-1, G-4, and G-8. The excellent agreement between the calculated and experimental profiles is illustrated by the normalized plots in Figs. 5.4 and 5.5.* Although it was initially hoped that the Mn^{54} distributions could be used to calculate the diameter of the cladding at each interim examination and possibly detect cladding swelling, the precision of the technique is not sufficient to detect the small changes expected.

*These are admittedly profiles with a minimum of scatter.

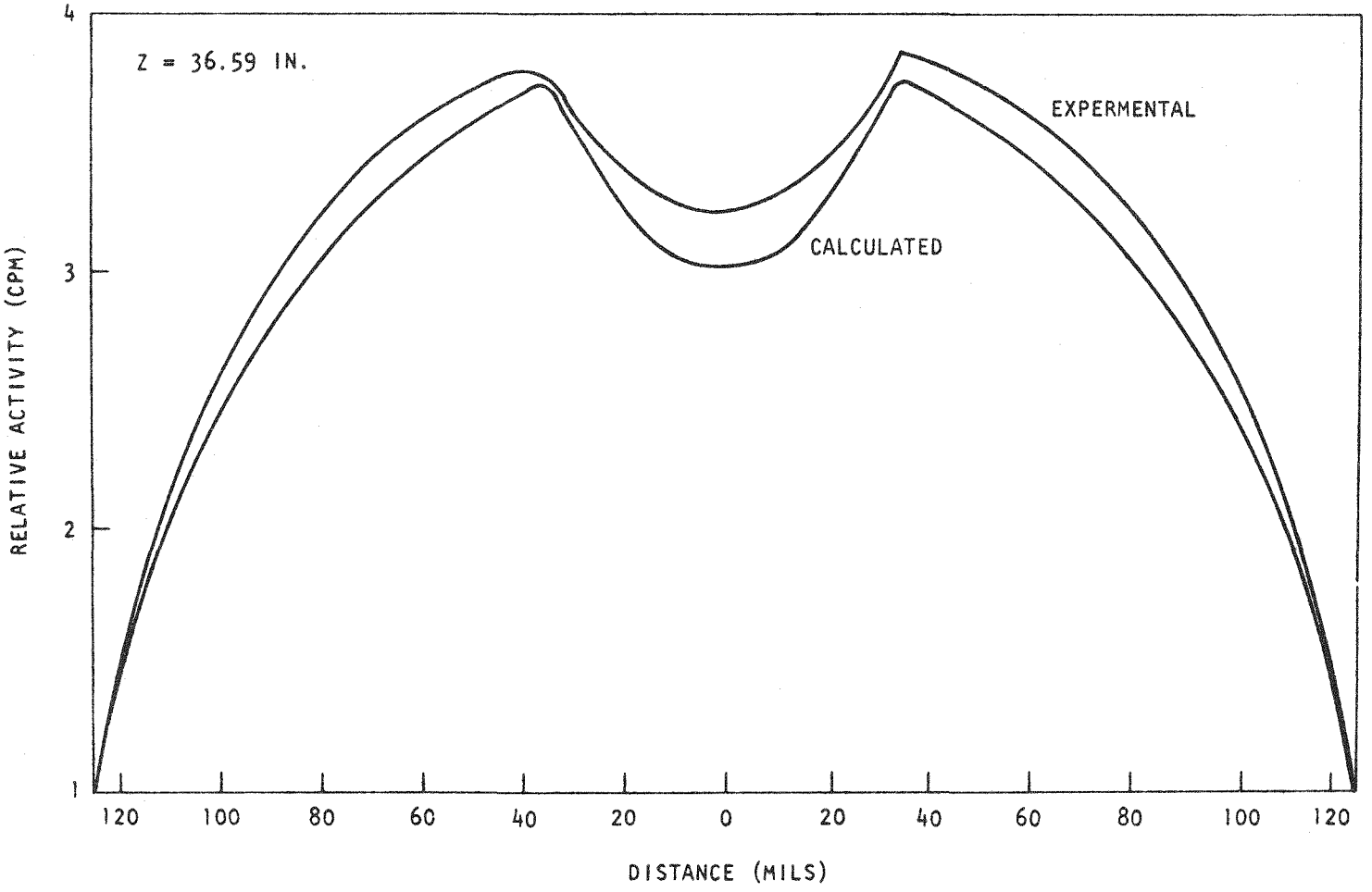

Fig. 5.1 Radial gamma scan of rod G-1 near upper fuel-blanket interface for Zr^{95}

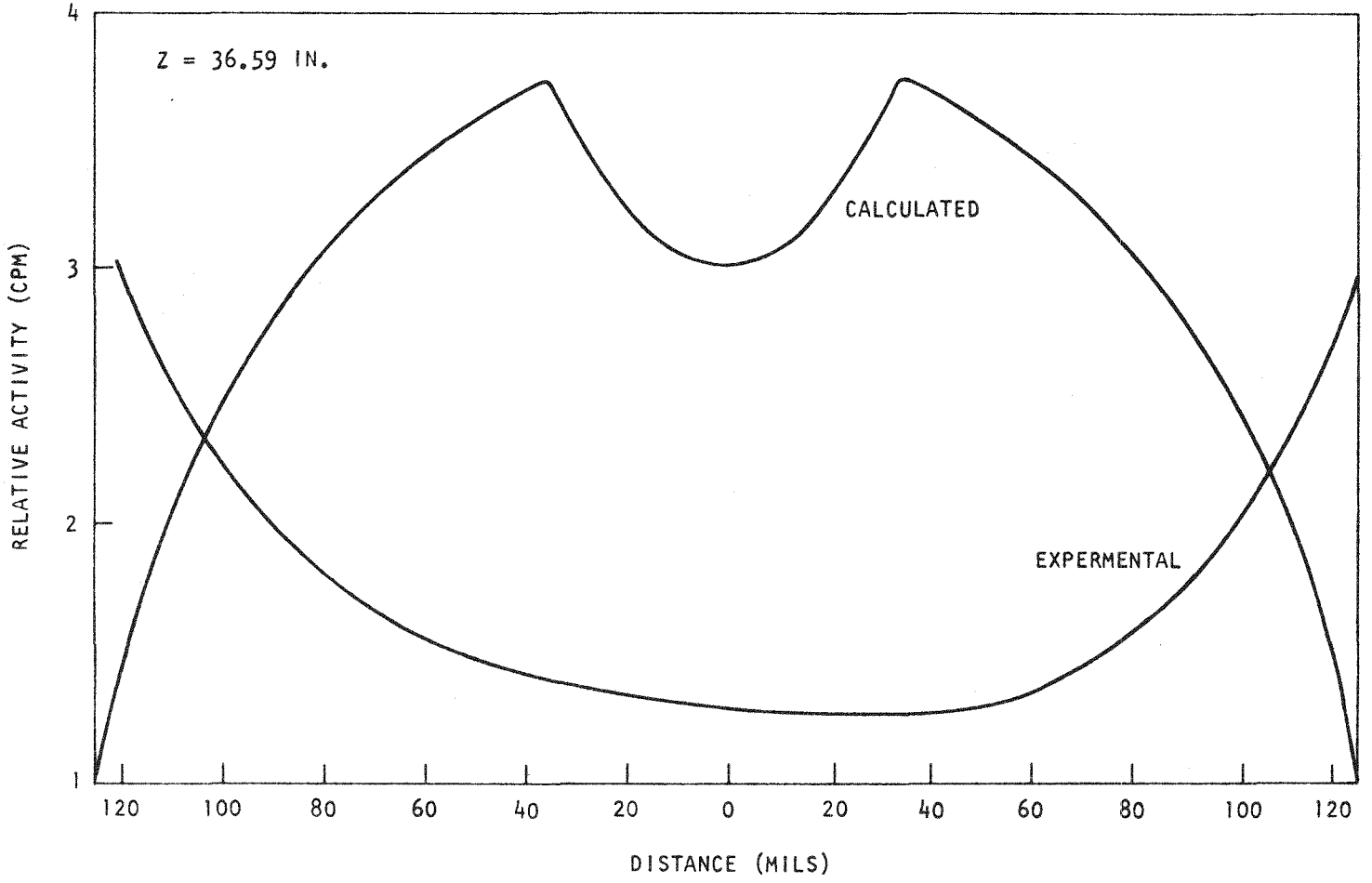

Fig. 5.2 Radial gamma scan of rod G-1 near upper fuel-blanket interface for I^{131}

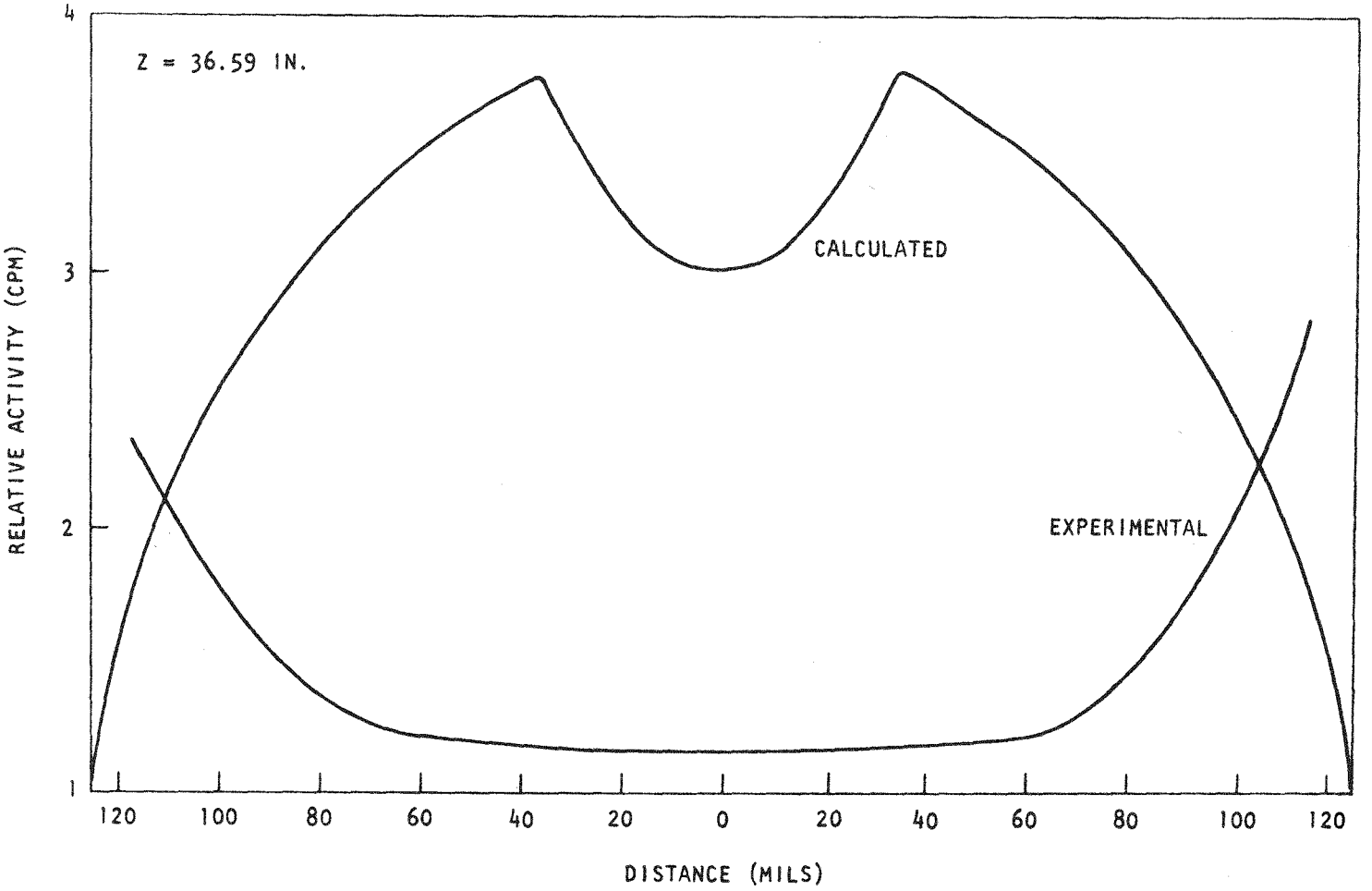

Fig. 5.3 Radial gamma scan of rod G-1 near upper fuel-blanket interface for Cs^{137}

Table 5.3

RADIAL SCANS OF Mn^{54} DISTRIBUTION IN COMPOSITE OF THREE STEEL TUBES SURROUNDING FUEL IN F-1 (XO94A) IRRADIATION

Rod Number	Location	Axial Position (in.)	Distance Between Highest Activity Levels (in.)					
			Outer Cladding		Thermal Barrier		Fuel Cladding	
			Measured	Calculated	Measured	Calculated	Measured	Calculated
G-1	Upper fuel-blanket interface, fuel region	36.59	0.710	0.728	0.370	0.388	0.270	0.268
G-1	Upper fuel-blanket interface, blanket region	37.59	0.725[a]	0.728	0.370	0.388	0.270	0.268
G-1	Upper fuel-blanket interface, blanket region	38.59	0.730	0.728	0.400	0.388	0.280	0.268
G-4	Upper fuel-blanket interface, fuel region	36.59	0.720	0.728	0.450	0.428	0.270	0.268
G-4	Upper fuel-blanket interface, blanket region	37.59	0.720	0.728	0.430	0.428	0.270	0.268
G-8	Below lower fuel-blanket interface	23.21	0.740	0.728	0.470	0.448	0.280	0.268

[a]Denotes an extrapolated value.

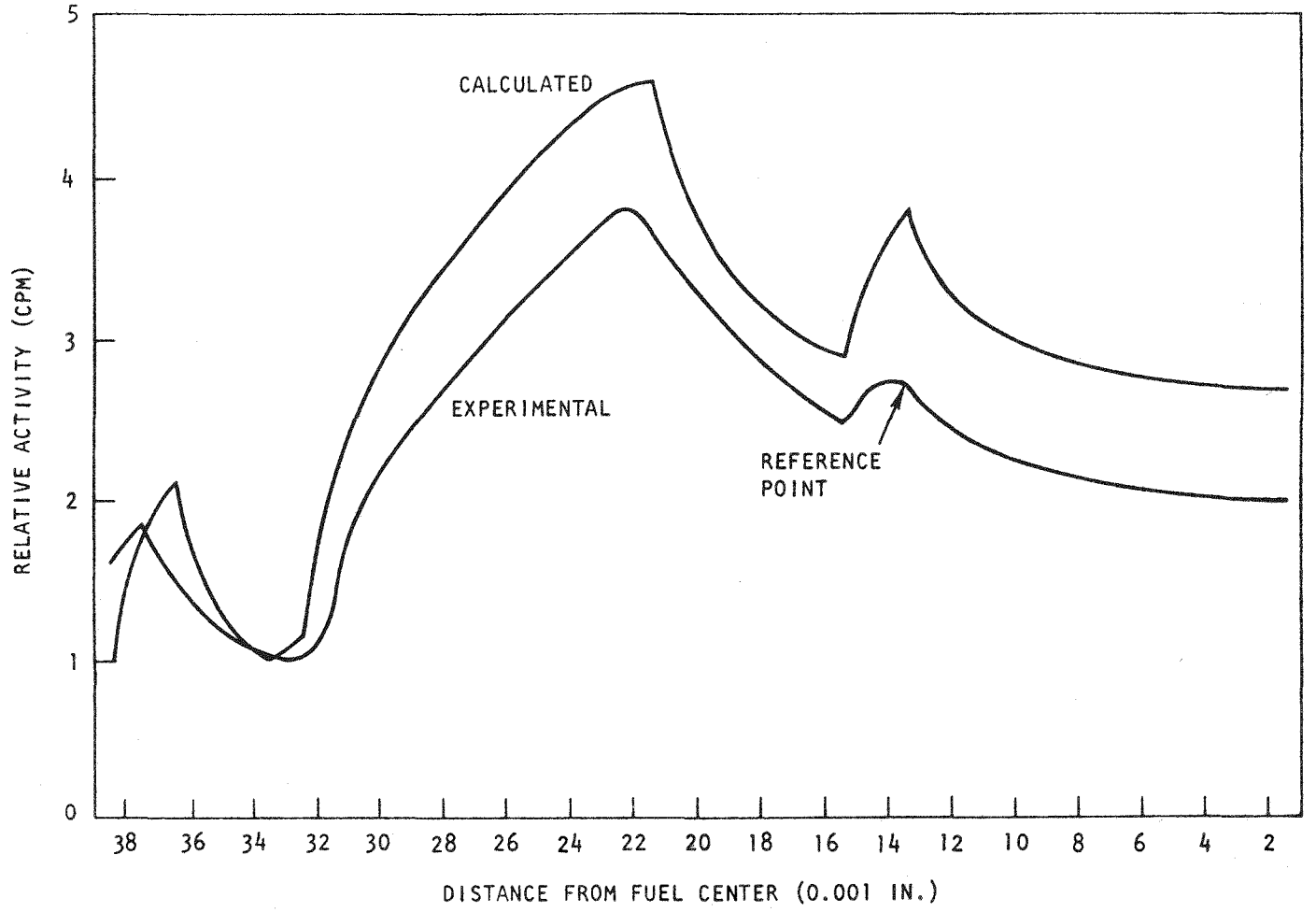

Fig. 5.4 Distribution of Mn^{54} in composite of three steel tubes surrounding fuel rod G-4 (axial position at 36.59 in.)

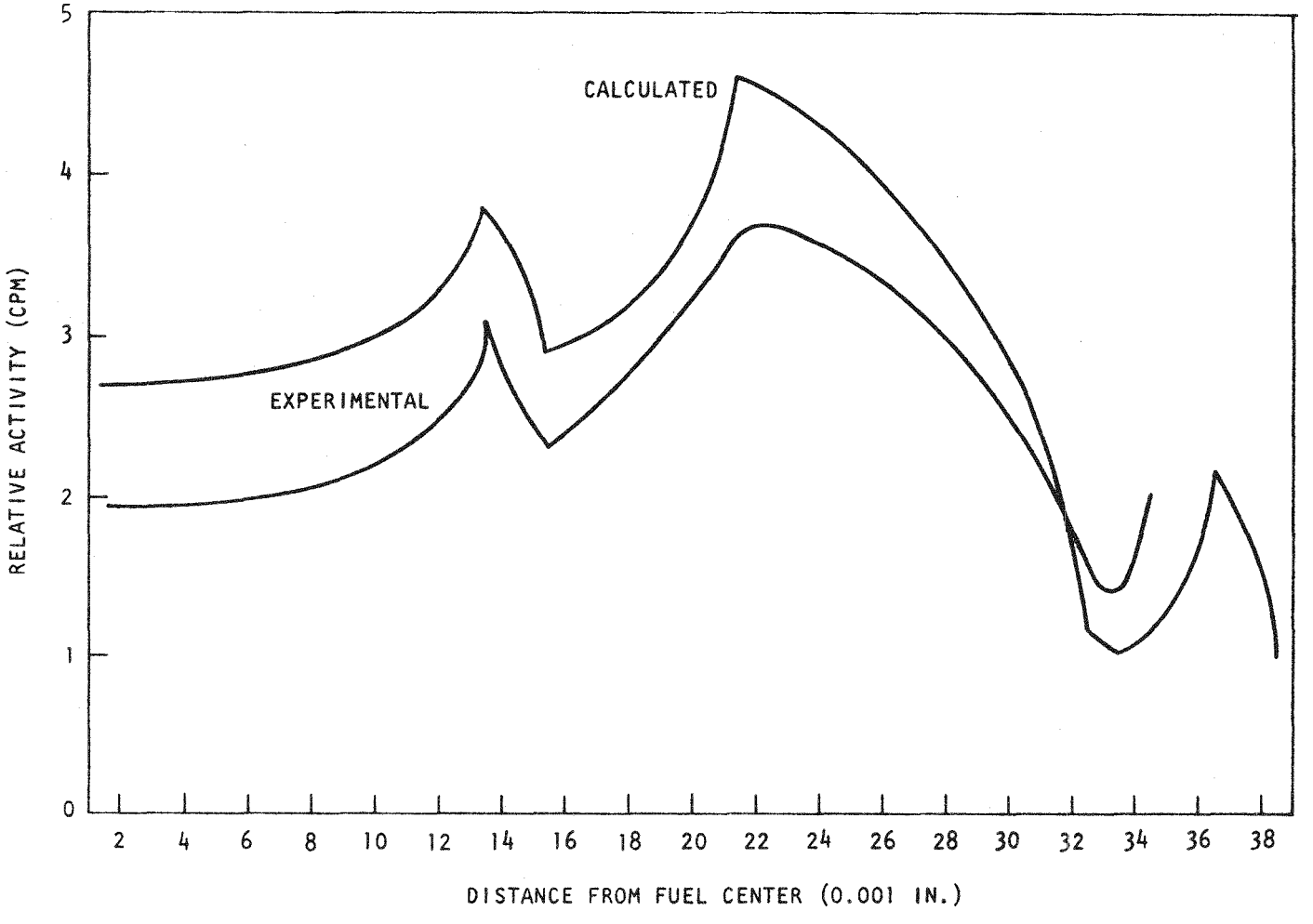

Fig. 5.5 Distribution of Mn^{54} in composite of three steel tubes surrounding fuel rod G-4 (axial position at 36.59 in.)

Supplemental gamma-scanning of several of the fuel rods was carried out during August 1973. Rod G-8 was scanned over its entire length at 0.5-in. intervals to provide an axial flux profile of the F-1 (XO94A) assembly in its new location (7B4) in the EBR-II. These data will be compared with similar axial scans made on rods G-3 and G-4 during the 25,000 MWd/Te examination when the subassembly was at the 7B6 location in EBR-II.

Gamma-scanning of rods G-4, G-6, and G-7, which contained active charcoal traps, was also carried out. These scans detected Cs^{137} and Cs^{134} in the charcoal traps. The presence of Cs^{134} was expected since this isotope is transported to the trap as Xe^{133}, which decays to Cs^{133} (stable). The Cs^{133}, in turn, is activated in (n, γ) reactions to Cs^{134}. The presence of Cs^{134} has been reported previously,[2] but the detection of Cs^{137} is new.

The distributions of Cs^{134} and Cs^{137} in the active charcoal traps of rod G-7 are shown in Figs. 5.6 and 5.7. Also shown are the preirradiation location and the present location of the charcoal in the active traps as determined from the neutron radiographs of the capsules. The charcoal has experienced a volumetric shrinkage of approximately 50% at this point in the irradiation. (Approximately one-half of the observed shrinkage occurred during the initial 25,000 MWd/Te exposure.) Partially as a consequence of the shrinkage, the stainless steel screens that divided the charcoal into axial sections have shifted toward the bottom of the capsule. This has resulted in an axial relocation of the charcoal within the original boundaries of the trap. Some of the charcoal in the lower trap is now a greater distance from the fuel and some of the charcoal in the upper trap is closer to the fuel.

The distribution of Cs^{134} shown in Figs. 5.6 and 5.7 correlates quite well with the location of the charcoal as determined from the neutron radiographs. In contrast, the distribution of Cs^{137} appears to be essentially uniform throughout the entire trap region. This behavior is not understood at the moment but may be related to the Cs^{137} background in the air cell at the Hot-fuel Examination Facility at EBR-II. This phenomenon is still under investigation.

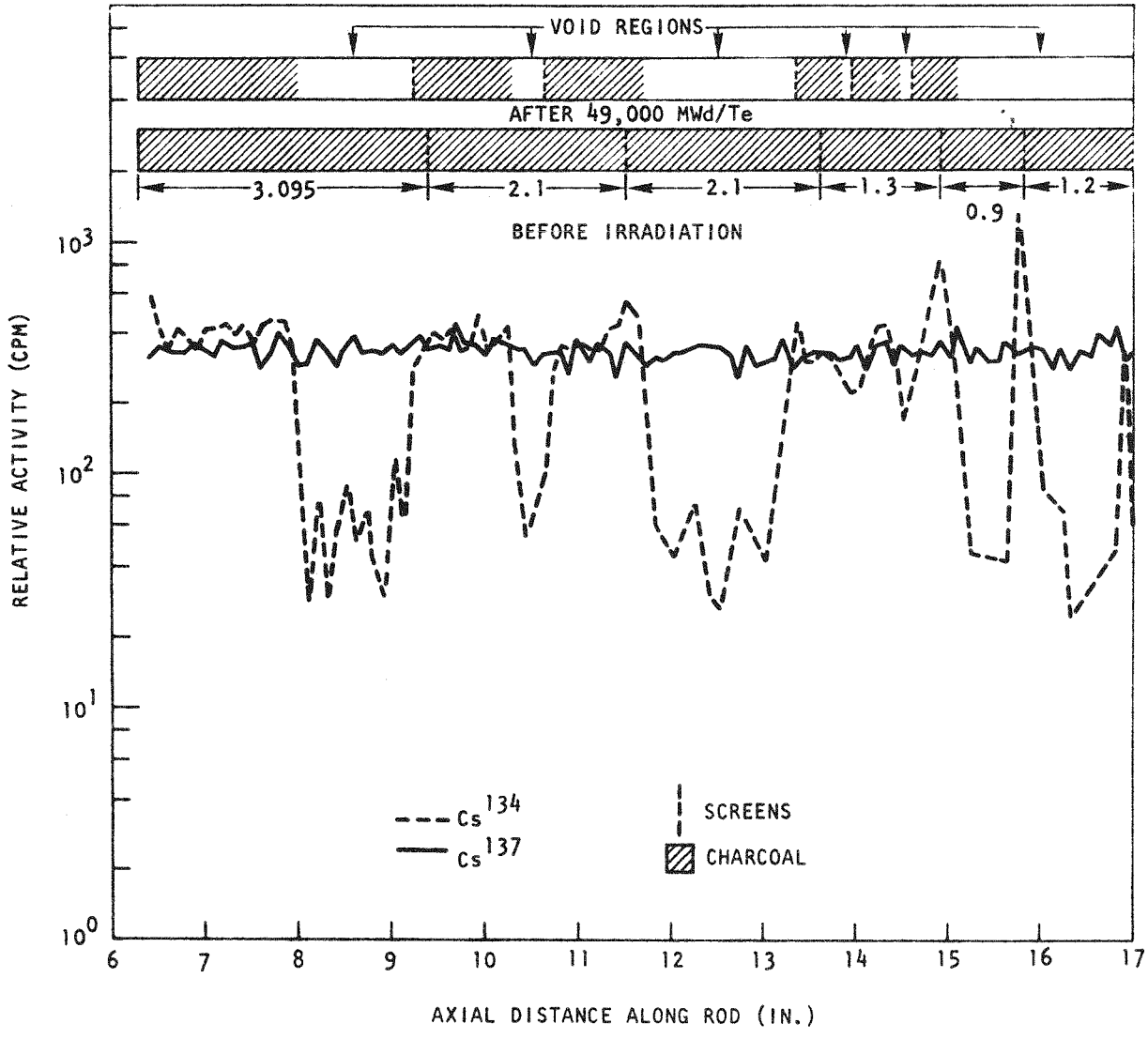

Fig. 5.6 Lower charcoal trap region in rod G-7

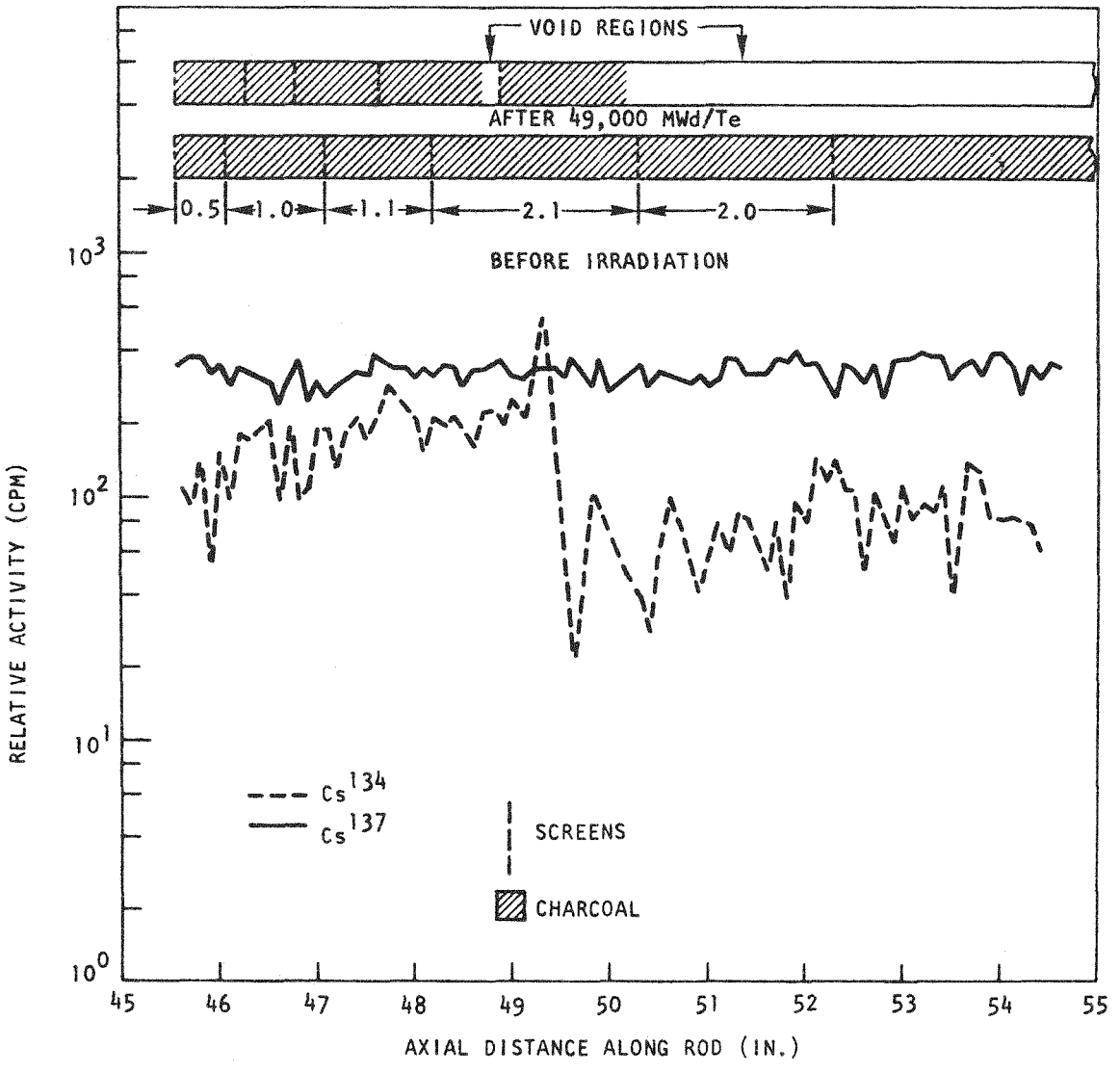

Fig. 5.7 Upper charcoal trap region in rod G-7

Samples of the cladding of the G-3 fuel rod were received in the irradiation material (primarily material from capsule GB-9) shipped to GGA from ANL-East. These cladding samples are being used in experiments to determine the actual operating temperature during irradiation using the Kr^{85} annealing technique discussed in the previous quarterly report.[3]

Cladding specimens from the center and both ends of the fuel column were examined by the Kr^{85} annealing technique. Preliminary estimates of the cladding temperature indicate that the G-3 rod may have operated 40°C below calculated values. Efforts are in process to secure a more definite temperature based on actual fission rates. Since the temperature determined by the annealing technique is the cladding inner temperature, corrections need to be applied to the measured values for comparison with the reference temperature. Applied corrections, such as the temperature differential across the cladding, and the circumferential correction normalize the data to the outer cladding surface facing the reactor core. These corrections are currently subject to a number of uncertainties which are being reevaluated.

The cladding specimens taken from the GB-9 fuel rod where the cladding temperature was measured by means of chromel-alumel thermocouples were examined by the annealing technique in an effort to confirm the method. However, the upper section of the GB-9 cladding is subject to a rather large circumferential temperature correction, which introduces substantial error. Additionally, the axial orientation of the specimen is unknown. Specimens from the mid-section or lower section of the cladding are available and will be examined. These areas have more nominal correction factors and may resolve the difficulty in assigning temperature end points.

Plenum-gas analysis and volume measurements have been made by ANL on the G-3 fuel rod. In addition, photomicrographs of the fuel cross section and the capsule-tube-to-end-fitting braze were taken and fuel density determinations were prepared by ANL. The results of the gas volume measurements indicate that the G-3 plenum volume was approximately the same as calculated. The photomicrographs of the capsule fuel tube to end fitting braze (nicro braze 50) indicated a sound joint and some minor sensitization and surface cracking. An archive sample or photomicrographs will be obtained from ORNL

for comparison. Postirradiation G-3 fuel densities were reported to have averaged in the range of 80% to 90% except in the region of the central hole at the top and bottom of the fuel column where the vapor-transported fuel density is about 60%.

5.2.2. Fast-flux Irradiation Experiment F-3

Work continued on the fabrication and assembly of the F-3 fast-flux experiment, which has been designed for irradiation in an EBR-II core position (row 4) and which will share a type J19A subassembly with an ANL Group-08 high-temperature chemistry experiment. The initial loading of the subassembly will contain ten F-3 fuel-rod capsules and nine Group-08 fuel-rod capsules. The F-3 fuel rods will achieve neutron exposures up to ~1.5 x 10^{23} nvt at 100,000 MWd/Te burnup. The F-3 fuel-rod cladding temperatures will range from 675°C to 750°C and the linear heat-generation ratings will range from 12 to 15 kW/ft.

Some changes were made in the design of the F-3 fuel-rod capsules during this period.

A minor modification to the lower rod end fittings of fuel rods G-16 and G-17 was made to facilitate their incorporation into a transient test assembly after irradiation is completed in EBR-II. Subcapsules containing neutron shield materials samples were fabricated and sent to ANL-East for inclusion into rods G-14, G-19, G-20, G-24, G-25, and G-26. The shield materials to be irradiated are ZrH_2 (1.6 H to metal), ZrH_2(1.75), Be, and BeO. These materials are contained in separate stainless-steel capsules and will be placed in part of the lower plenum of the rods that will be irradiated to an exposure of 50,000 MWd/Te. (The new GCFR reference design includes neutron shield material in the upper end of the fuel rods to shield the core-support grid plate to a maximum neutron fluence of 8 x 10^{21} n/cm^2 over a 30-yr life.)

Planning is continuing on the inclusion of sealed thermocouple segments in the flow strips for the F-3 J19 subassembly. Trial fabrication at GGA of these flow strips has started.

Fuel cladding tubes roughened mechanically by Alpha Engineering were received and four of six tubes were found to be suitable for use in the F-3 experiment. The tubes roughened by Superior Tube are ready for shipment to GGA.

During oxygen-to-metal ratio adjustment from 1.98 to 1.94 on fuel pellets at ANL-East, additional fuel sintering and densification occurred. This resulted in a fuel-cladding diametral gap increase of about 0.0025 in. over the specified gap of 0.0035 in. The effect of this larger gap was analyzed for an EBR-II startup using the LIFE-II code. It was found that no part of the fuel would melt under the design conditions even with the increased fuel-cladding gap. An analysis of HEDL P-19 data[4] for power to melt also indicates that the densified fuel pellets will operate below center melting at the design power levels. Discussions are being held with ANL-East concerning the thermal performance of the Group-08 fuel rods, which will share the J19 subassembly and the input parameters that are to be used for the thermal analysis of the full 19-rod subassembly using the HECTIC code.

The assembly of one fuel rod (except the xenon tagging) for the F-3 experiment has been completed by ANL-East. Completion of the fabrication of the F-3 fuel-rod capsules is now scheduled for early 1974.

REFERENCES

1. "Gas-Cooled Fast Breeder Reactor Quarterly Progress Report for the Period May 1, 1972 through July 31, 1972," USAEC, Report, Gulf-GA-A12252, Gulf General Atomic, August 31, 1972.

2. "Gas-Cooled Fast Breeder Reactor Quarterly Progress Report for the Period February 1, 1973 through April 30, 1973," USAEC, Report Gulf-GA-A12635, Gulf General Atomic, June 15, 1973.

3. "Gas-Cooled Fast Breeder Reactor Quarterly Progress Report for the Period May 1, 1973 through July 31, 1973," USAEC, Report Gulf-GA-

A12728, Gulf General Atomic, October 10, 1973.

4. Leggett, R. D., et al., "Linear Heat Rating for Incipient Fuel Melting in UO_2-PuO_2 Fuel," Trans. Am. Nucl. Soc., Vol. 15, No. 2, November 1972, p. 752.

6. TASK 4700—NUCLEAR ANALYSIS AND REACTOR PHYSICS

6.1. GCFR CRITICAL EXPERIMENT PLANNING

Meetings were held with the Reactor Physics Branch, Division of Reactor Research and Development (DRRD), and the Applied Physics Division at Argonne National Laboratory to discuss the proposed GCFR critical experiment program. The topical report describing this proposed program was subsequently published and distributed.[1]

A draft of a preliminary work plan for the first critical assembly was prepared by the ANL Applied Physics Division. An initial review has been made by the GCFR Physics Group at GGA and comments have been forwarded to ANL. Joint planning with ANL for the first assembly is continuing.

6.2. LMFBR CRITICAL ASSEMBLY SURVEILLANCE

6.2.1. Reanalysis of ZPPR-2 Central Worths with ENDF/B Version 3 Cross Sections

The availability of ENDF/B Version 3 cross sections prompted a re-examination of the central worths in the voided inner core of ZPPR-2. The first-order-perturbation worths were calculated using the real and adjoint fluxes generated previously (using ENDF/B Version 2 cross sections) with the two-dimensional code ADGAUGE and the perturbation code STOER. Appropriate sample cross sections were generated in a homogeneous GGC-5 cell representation. The effect on central worths of extending the resolved resonance treatment in the GAROL section of GGC-5 from 3 keV to 7.1 keV was also examined. Version 2 and Version 3 results, including some minor corrections to the earlier results,[2] are compared in Table 6.1.

With the exception of the B-1 boron sample, small-sample correction factors and flux distortion factors have not been applied. Consideration

Table 6.1

COMPARISON OF MEASURED AND CALCULATED[a] CENTRAL WORTHS

FOR THE 93-DRAWER VOIDED PLATE ZONE OF ZPPR-2

Sample	Composition	Version 2 Calculated Worth[b] (Ih/kg)	Version 3 Calculated Worth[c] (Ih/kg)	Version 3 Calculated Worth[d] (Ih/kg)	Experimental Worth[e] (Ih/kg)	C (7.10 keV)/E
B-1	B-10	-1286	-1296	-1313	-1314	1.00
Fe-1	Fe	-3.22	-4.07	-4.07	-3.55	1.15
U-6	93% U-235	105.9	104.5	104.1	81.6	1.28
DU-6	U-238	-7.31	-7.31	-7.37	-6.01	1.23
Pu-30	Pu-239	131.8	136.9	136.6	117.6	1.16
Pu-48	41% Pu-239	85.3	87.2	87.0	73.7	1.18
C-1	Carbon	-21.3	-20.1	-20.1	-17.5	1.15

[a] 1% $\Delta k/k$ = 1015.7 Ih.

[b] ENDF/B Version 2 (modified) cross sections for all except boron and iron.

[c] GAROL treatment of resolved resonance region up to 3.35 keV.

[d] GAROL treatment of resolved resonance region up to 7.10 keV.

[e] R. G. Palmer, Argonne National Laboratory (private communication).

of these factors is expected to result in less than a 1% increase in the calculated worths of the uranium samples and about 6 to 7% increase in the calculated worths of the plutonium samples.

A significant change is noted in the Fe-1 sample worth, which now displays the expected "central-worth discrepancy." Improvement in other central worths is marginal.

The suitability of the voided inner core of ZPPR-2 as a modelling region for measuring GCFR central worths was also reinvestigated. The comparative median flux energies for this assembly as compared to GCFR and other plutonium criticals of interest are given in Table 6.2. The normalized spectra for the first three fluxes in Table 6.2 are shown in Fig. 6.1. Both Table 6.2 and Fig. 6.1 are derived from 156-group spectrum calculations using the SDX code.[3]

6.2.2. Effect of GAROL Extension from 3.3 keV to 7.1 keV.

A brief study of the effect of extending the GAROL treatment of the resolved resonance region to higher energies was carried out. The effect of the extension on the absorption resonance integrals for the primary nuclides in the voided inner core of ZPPR-2 is indicated in Table 6.3.

For each of the heavy metals (except U^{235}, for which no unresolved GANDY parameters were generated), the extension of the GAROL calculation increases the resolved resonance integral and, of course, decreases the unresolved resonance integral since it covers less range. The total resonance integral for the heavy metals decreases slightly. However, the resolved integrals for the structural nuclides iron, chromium, and nickel increase markedly with no corresponding decrease in the unresolved region integrals. The net effect is a decrease in the eigenvalue. This effect is observed in the following eigenvalue calculations for a spherical homogeneous benchmark model of ZPR-6, Assembly 7.[4]

Table 6.2

COMPARATIVE MEDIAN FLUX ENERGIES

Reactor	Region	Spectrum Calculation	Median Flux (keV)
GCFR	Core zone 1	Space dependent	174.8
GCFR	Radial blanket	Space dependent	137.7
ZPPR-2	Voided inner core	Fundamental mode	171.6
ZPPR-2	Voided inner core	Space dependent	169.1
ZPPR-2	Normal inner core	Space dependent	142.5
ZPR6-7	Normal core	Fundamental mode	141.0
ZPR6-7	High-240 zone	Fundamental mode	147.9
ZPR6-7	Voided high-240	Fundamental mode	180.0

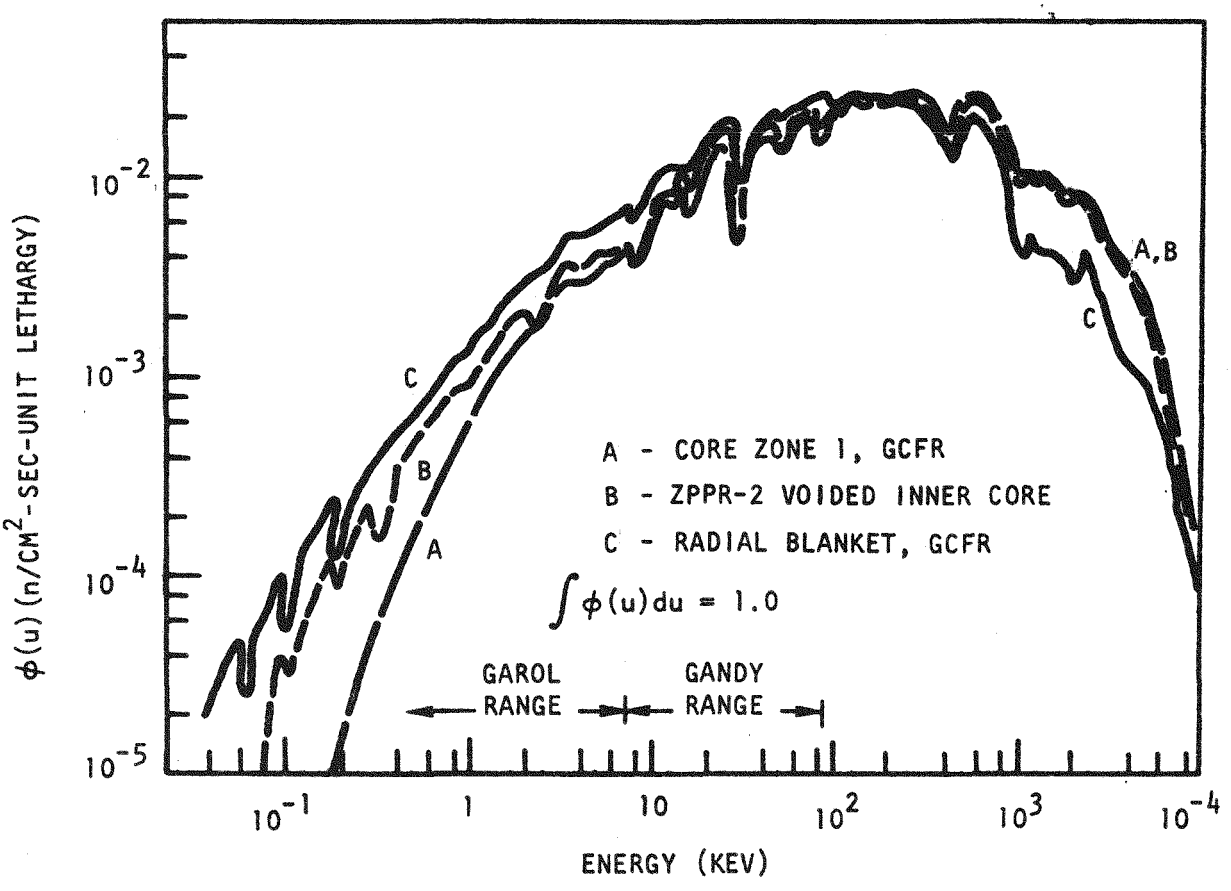

Fig. 6.1 Comparison of spectra for GCFR core zone 1 and radial blanket with ZPPR-2 voided inner core

Table 6.3

ABSORPTION RESONANCE INTEGRALS FOR ZPPR-2 VOIDED INNER CORE

Nuclide	GAROL to 3.35 keV			GAROL to 7.10 keV		
	Resolved	Unresolved	Total	Resolved	Unresolved	Total
O	2.057×10^{-7}	-------	2.057×10^{-7}	2.867×10^{-7}	-------	2.867×10^{-7}
Cr	6.318×10^{-3}	-------	6.318×10^{-3}	2.587×10^{-2}	-------	2.587×10^{-2}
Fe	1.008×10^{-2}	-------	1.008×10^{-2}	1.206×10^{-2}	-------	1.206×10^{-2}
Ni	6.372×10^{-3}	-------	6.372×10^{-3}	1.224×10^{-2}	-------	1.224×10^{-2}
U^{235}	2.923	-------	2.923	4.030	-------	4.030
U^{238}	2.873×10^{-1}	1.125	1.412	4.725×10^{-1}	8.632×10^{-1}	1.336
Pu^{239}	2.407	4.258	6.665	3.287	2.906	6.193
Pu^{240}	7.934×10^{-1}	1.378	2.171	1.022	9.795×10^{-1}	2.001
Pu^{241}	3.027	7.915	1.049×10^{1}	4.216	5.983	1.020×10^{1}
Pu^{242}	6.842×10^{-1}	4.632×10^{-1}	1.147	8.090×10^{-1}	2.630×10^{-1}	1.072

k_{eff} (GAROL to 3.35 keV) 0.9887

k_{eff} (GAROL to 7.10 keV) 0.9838

Δk 0.0049

6.3. METHODS DEVELOPMENT

Development of analytical methods during this quarterly period was concerned with the following items:

The ADGAUGE two-dimensional diffusion code, which presently is the only GGA diffusion code with first-order-perturbation capability, was modified to allow a previous flux guess as a restart option. An initial test of this option showed a significant time savings in iterations on eigenvalues.

The one-dimensional transport perturbation code GAPER-1D was modified to utilize output real and adjoint flux tapes from an improved, fast-running version of the transport code 1DFX.

Data tapes with ENDF/B Version 3 cross sections were prepared in the GAR format for use in the GAROL section of GGC-5 at temperatures of 1300°K and 3000°K. These were necessary for evaluation of the hot eigenvalue and Doppler calculations of the 300-MW(e) GCFR.

The GAROL option in GGC-5 was modified to allow resolved resonance treatments to 7.10 keV from the previous upper limit of 3.35 keV (as discussed previously).

REFERENCES

1. Moore, R. A., "A Critical Experiment Program for the 300-MW(e) Gas-Cooled Fast Breeder Reactor—Scope and Purpose," USAEC, Report Gulf-GA-A12780, Gulf General Atomic, October 17, 1973.

2. "Gas-Cooled Fast Breeder Reactor Quarterly Progress Report for the Period August 1, 1972 through October 31, 1972," USAEC, Report Gulf-GA-A12421, Gulf General Atomic, December 8, 1972.

3. Stacey, W. M., Jr., et al; "SDX—An Intermediate-Group, Spatially-Dependent Capability for the Preparation of Fast Neutron Multigroup Cross Sections," USAEC, Report ANL-8010, Argonne National Laboratory (to be published).

4. Till, C. E., et al; "ZPR-6 Assemblies 6A and 7: Benchmark Specifications," USAEC, Report ANL-7910, Argonne National Laboratory, January 1972, p. 86.

Appendix
PUBLICATIONS

"A Critical Experiment Program for the 300-MW(e) Gas-Cooled Fast Breeder Reactor—Scope and Purpose," R. A. Moore, USAEC, Report Gulf-GA-A12780, October 17, 1973.

"GCFR Pressure Equalization System Development Plan," R. J. Campana and A. F. Weinberg, USAEC, Report Gulf-GA-A12471, October 30, 1973.